

31. ISOTOPE GEOCHEMISTRY OF NINETYEAST RIDGE BASEMENT BASALTS: SR, ND, AND PB EVIDENCE FOR INVOLVEMENT OF THE KERGUELEN HOT SPOT¹

D. Weissel² and F. A. Frey³

ABSTRACT

The Ninetyeast Ridge lavas have Sr and Nd isotopic ratios intermediate between those of Indian Ocean MORBs and those of the very enriched Kerguelen hot spot. In an Nd-Sr isotope diagram, they also plot close to the fields of St. Paul Island lavas and of the early magmatism on Kerguelen Archipelago. The Ninetyeast Ridge lavas were generated by mixing among at least three components: a depleted, MORB-type component, such as the one erupted today on the Southeast Indian Ridge; a very enriched, high-⁸⁷Sr/⁸⁶Sr, low- ϵ_{Nd} , OIB-type component (the Kerguelen hot spot); and an OIB-type component comparable to that sampled from the St. Paul (and Amsterdam) lavas. The Ninetyeast Ridge lavas show a typical Dupal anomaly signature and Pb, Sr, and Nd isotopic systematics indicate that the Kerguelen hot spot was involved in the ridge's formation as the Indian plate moved northward.

The different sites cored during ODP Leg 121 show a trend in their isotopic compositions, from less radiogenic ²⁰⁶Pb/²⁰⁴Pb ratios and intermediate ⁸⁷Sr/⁸⁶Sr and ¹⁴³Nd/¹⁴⁴Nd ratios in the oldest lavas (Site 758) toward more radiogenic ²⁰⁶Pb/²⁰⁴Pb, higher ϵ_{Nd} , and lower ⁸⁷Sr/⁸⁶Sr values in the youngest lavas (Site 756). The lavas from Site 757 have ²⁰⁶Pb/²⁰⁴Pb ratios intermediate between those of the lavas from Sites 756 and 758 and higher ⁸⁷Sr/⁸⁶Sr and lower ϵ_{Nd} values. The relative proportions of the hot spot(s) and MORB component have evolved with time, reflecting differences of tectonic setting: the relative proportion of the Kerguelen hot spot component appears lower in the younger Site 756 lavas than in the older lavas from Sites 757 and 758. Site 756 coincides with the beginning of rifting at the Southeast Indian Ridge, about 43 Ma ago. The formation of the early Kerguelen Archipelago lavas may have drained most of the plume-derived material toward the Antarctic plate. Alternatively, the proximity of the spreading-ridge axis may account for the isotopic similarity of the Site 756 lavas to young lavas erupted on the Southeast Indian Ridge, from 33° to 37°S. The older lavas of Ninetyeast Ridge may have formed when the hot spot and ridge axis did not exactly coincide.

The involvement of the third component, a St. Paul hot spot, in the genesis of the Ninetyeast Ridge lavas, especially for the Site 756 lavas, is clearly indicated by Sr, Pb, and Nd isotope systematics and also by trace element ratios.

These data, together with those from the Kerguelen Plateau, indicate that the Kerguelen hot spot has been active more or less continuously in the South Indian Ocean for at least 115 Ma. This could indicate that the plume, and by inference the Dupal anomaly, is deep seated in origin.

INTRODUCTION

We present Sr, Pb, and Nd isotopic data for basalts from Ocean Drilling Program (ODP) Sites 756, 757, and 758 on Ninetyeast Ridge (Fig. 1). Major and trace element geochemistry and petrographic descriptions of these samples, and a few others, are discussed in the companion paper of Frey et al. (this volume). We focus in this paper on the interpretation of the isotopic data to understand the origin and evolution of Ninetyeast Ridge.

Marine magnetic and paleontological data (Shipboard Scientific Party, 1974a, 1974b) indicate that Ninetyeast Ridge is approximately contemporaneous with oceanic crust to the west; furthermore, the ridge is in local isostatic equilibrium (Bowin, 1973). These data suggest that Ninetyeast Ridge formed on either very young oceanic crust or at a spreading axis. The volume of magma generated to build a ridge with an average width of 200 km (Schlich, 1982) and more than 2 km in height requires a source of enhanced magmatism. The paleomagnetic data for basalts recovered during Deep Sea Drilling Project (DSDP) Legs 22 and 26 (Peirce, 1978) are consistent with eruption and cooling at a latitude of about 50°S, the approximate latitude of the Kerguelen-Heard Plume (presently under Heard Island, about 55°S). The formation of the ridge accompanied the rapid northward migration

of the Indian plate. The earliest recorded ridge activity is 81 Ma at DSDP Site 216 (Duncan, 1978), although Site 758 north of Site 216 is >80 Ma, and older material is probably buried beneath the Bengal Fan (Curry et al., 1982). Earlier magmatic activity possibly associated with the Kerguelen-Heard Plume is recorded by the Rajmahal Traps in northeast India; however, Mahoney et al. (1983) concluded that the Rajmahal Traps lavas were contaminated by continental lithosphere during ascent. The youngest activity at the southern end of Ninetyeast Ridge (DSDP Site 254, minimum age of 38 Ma; Duncan, 1978) was terminated by spreading at the Southeast Indian Ridge 43 to 36 Ma ago (east to west progression; Royer and Sandwell, 1989), when the Indian-Australian plate migrated northward away from the source of magmatism generating Ninetyeast Ridge.

Paleomagnetic, bathymetric, and geochemical data all support the idea that Ninetyeast Ridge formed above a mantle plume (Morgan, 1972; Luyendyk and Rennick, 1977; Peirce, 1978; Curry et al., 1982; Molnar and Stock, 1987). These data, together with plate reconstructions, strongly support the hypothesis that this was the Kerguelen-Heard Plume (Duncan, 1978; Whitford and Duncan, 1978). However, there is considerable uncertainty about the tectonic setting of the plume activity that was responsible for producing Ninetyeast Ridge; for example, was Ninetyeast Ridge created by a hot spot located on a spreading-ridge axis, like Iceland, or was the hot spot forming Ninetyeast Ridge north or south of the spreading axis? If the spreading axis was located north of the hot spot, Ninetyeast Ridge can be explained as a hot-spot trace on the Indian plate only if the spreading axis underwent a series of southerly ridge jumps or if the spreading was strongly asymmetric (Sclater and Fisher, 1974; Peirce, 1978). There is strong evidence for a major, southward ridge jump at 60

¹ Weissel, J., Peirce, J., Taylor, E., Alt, J., et al., 1991. *Proc. ODP, Sci. Results*, 121: College Station, TX (Ocean Drilling Program).

² Laboratoires Associés Géologie-Pétrologie-Géochronologie, Earth and Environment Sciences Department, Brussels Free University, CP 160, Avenue F. D. Roosevelt, 50, B-1050 Brussels, Belgium.

³ Department of Earth, Atmospheric and Planetary Sciences, Massachusetts Institute of Technology, Cambridge, MA 02139, U.S.A.

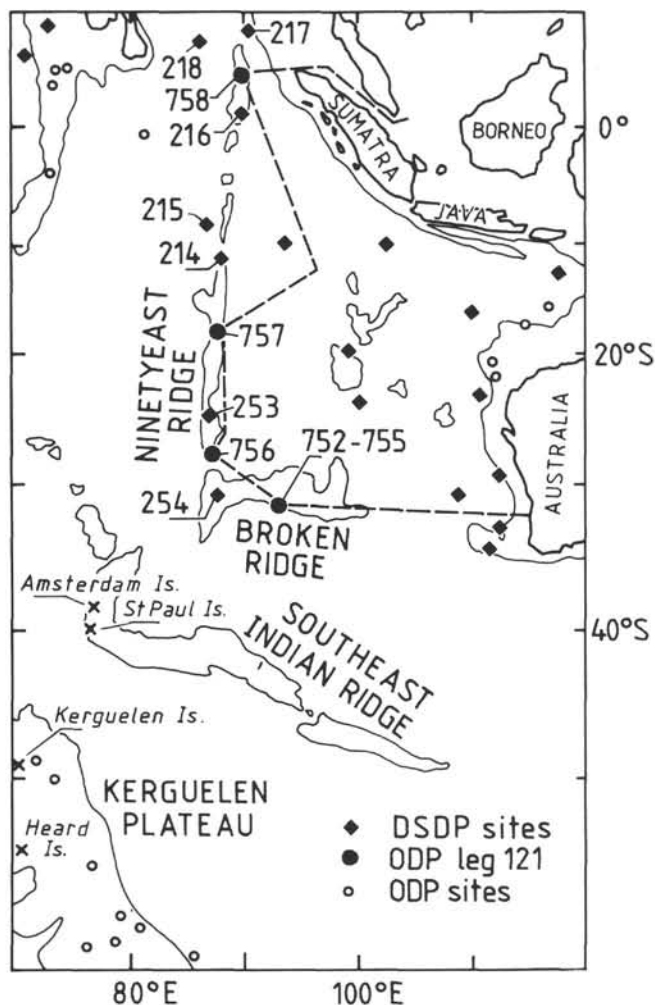


Figure 1. Location map of the East Indian Ocean showing Ninetyeast Ridge with DSDP and ODP sites and the various tectonic features relevant to this study. Modified from Peirce, Weissel, et al. (1989).

Ma (Royer and Sandwell, 1989; Peirce, Weissel, et al., 1989), which makes that scenario not unreasonable in this environment (Royer et al., this volume). Plume mantle, with a potentially high temperature, may control the position of the spreading axis segment west of the Ninetyeast Fault, with the result that the axis episodically migrated southward, despite the northward movement of the more westerly segments of the spreading axis. The reader is referred to Royer et al. (this volume) for a more detailed discussion of these questions.

The geochemistry of DSDP samples from Ninetyeast Ridge (Sites 214, 216, and 254; see review in Frey et al., 1977) shows them to be incompatible-element-enriched tholeiites, ferrotholeiites, and oceanic andesites (at Site 214 only). Surprisingly, there is little isotopic data for these lava samples (Sr and Pb data for two samples—Dupré and Allègre, 1983; Sr and Nd data for six samples—Mahoney et al., 1983). Only one sample (a basalt from Site 254) was analyzed for Sr, Nd, and Pb isotopes (Hart, 1988). Nevertheless, these isotopic data confirm that the Ninetyeast Ridge lavas are different from mid-ocean ridge basalts (MORBs) and isotopically broadly similar to the present Kerguelen Archipelago rocks (Dupré and Allègre, 1983; Mahoney et al., 1983). These data require a long-term, relatively incompatible-element-

enriched mantle⁴ source(s) and belong to the so-called Dupal anomaly, as defined by Hart (1984) on the basis of the observation of Dupré and Allègre (1983) that oceanic island basalts (OIBs) of the southern Indian and Pacific oceans usually show higher $^{87}\text{Sr}/^{86}\text{Sr}$, lower $^{143}\text{Nd}/^{144}\text{Nd}$, and higher $^{207}\text{Pb}/^{204}\text{Pb}$ and $^{208}\text{Pb}/^{204}\text{Pb}$ ratios for a given $^{206}\text{Pb}/^{204}\text{Pb}$ value in comparison with basalts from the North Atlantic and Pacific oceans. Most basalts from the Kerguelen Archipelago (Dosso et al., 1979; Dosso and Murthy, 1980; White and Hofmann, 1982; Storey et al., 1988; Weis et al., 1989b; Gautier et al., 1990), Kerguelen Plateau (Davies et al., 1989; Weis et al., 1989a), and Heard Island (Barling et al., 1988; Storey et al., 1988) have even more enriched isotopic signatures (i.e., higher $^{87}\text{Sr}/^{86}\text{Sr}$, lower ϵ_{Nd} , and higher $^{207}\text{Pb}/^{204}\text{Pb}$ and $^{208}\text{Pb}/^{204}\text{Pb}$), especially the most differentiated lavas of the Kerguelen Archipelago (Gautier et al., 1989), which may constitute the purest composition of the Kerguelen hot spot. Because the Ninetyeast Ridge lavas plot, on average, in all incompatible trace element diagrams and isotope diagrams in a position intermediate between a typical depleted component (N-MORB) and a very enriched OIB-type component, which may be the Kerguelen hot spot, Ninetyeast Ridge may have been formed by mixing between these two components (Weis et al., 1991). If this hypothesis is correct, it would help confirm that Ninetyeast Ridge forms a major portion of the 120-Ma (Leclaire et al., 1987) plume trace caused by the Kerguelen-Heard Plume.

The main goals of this paper are to establish the isotopic characteristics of the magmas forming the Ninetyeast Ridge lavas (i.e., the isotopic characteristics of their mantle sources) and to compare them with those of the Kerguelen Archipelago and Kerguelen Plateau basalts and other Indian Ocean basalts. By studying lavas of different ages along Ninetyeast Ridge, we should be able to infer not only the source components required but how the relative proportions of these components changed with time. Because the data for basalts from the Kerguelen Archipelago define an extreme isotopic component in diagrams of oceanic mantle-derived rocks (e.g., White, 1985; Zindler and Hart, 1986), the study of basalts from Kerguelen and Heard islands, Ninetyeast Ridge, and the Kerguelen Plateau provides a unique opportunity to investigate the characteristics (in terms of geochemistry, geography, distribution, and origin) and evolution of a very long-lived mantle plume of unusual composition (≈ 120 Ma; Davies et al., 1989; Weis et al., 1989a).

SAMPLE SELECTION AND PREPARATION

Samples were carefully selected to obtain the least altered, representative lavas of the major flow units at each site. The initial selection was made aboard ship on the basis of thin-section observation and compositional data obtained by shipboard X-ray-fluorescence (XRF) analysis. A total of 122 samples was chosen for study, and 72 samples were analyzed for major and trace elements (see companion paper of Frey et al., this volume). Finally, 41 samples (see Table 1) were selected for isotopic analysis on the basis of major and trace element data, but also to include the different petrographic units (which resulted in the selection of 10 samples for Site 756, 13 for Site 757, and 18 for Site 758).

For Sr and Nd isotopic analyses, the samples were leached in acid to remove secondary alteration phases. Two processes, differing essentially in the temperature of the acid, were used. Two splits of Sample 121-757C-9R-1 (Piece 3, 105–109 cm) were

⁴ Enriched and depleted are used in this paper relative to bulk earth for Sr and Nd isotopes and relative to the Northern Hemisphere reference line (NHRL; Hart, 1984) for Pb isotopes.

processed, once with warm acid leaching, once with "cold"⁵ acid leaching, and relatively close values for $^{87}\text{Sr}/^{86}\text{Sr}$ ratios were obtained (see Table 3), although a slightly higher value was obtained with the cold leaching procedure. The initial weights of the powders varied between 300 and 500 mg. Quartz-distilled 6 N HCl was added to the powder, in a proportion of 1.5 mL for 150 mg. The mixture was put in a Teflon beaker in an ultrasonic bath for 10 min and left to sit overnight. After another 10 min in the ultrasonic bath, the beaker was heated to 40°C for about 2 hr. After heating, the mixture was returned to the ultrasonic bath for 10 min, and then the powder was allowed to settle for 15 min and the acid was collected with an Eppendorf-type pipette and stored in a polypropylene bottle. A new batch of 6 N HCl was added to the remaining powder and the same cycle, 10 min in the ultrasonic bath, 2-hr heating to 40°C, and 10 min in the ultrasonic bath, was repeated until the yellow (Fe) color of the leaching solution was almost gone. This usually required five to six cycles. For the cold leaching, the procedure was similar, except that no heating step was involved. Samples 1 through 11 were treated by a cold acid leaching and samples 12 through 41 were processed by a warm acid leaching.

The results of the warm acid leaching (samples 12 through 41), which were initially selected because the procedure appeared more efficient in reducing $^{87}\text{Sr}/^{86}\text{Sr}$ related to alteration, were very surprising in the sense that higher $^{87}\text{Sr}/^{86}\text{Sr}$ values were obtained for the leached samples than for the unleached samples. To solve that problem, Samples 121-757C-9R-8 (Piece 4A, 54–59 cm) and 121-758A-70R-2 (Piece 7F, 129–133 cm) were processed through different acid-leaching procedures: a cold leaching (samples 1 through 11), a mildly warm leaching, a warm leaching (initial processing for samples 12 through 41), and a leaching following Mahoney's (1987) procedure (i.e., cold acid leaching with elimination of the fines by removing the acid immediately [<3 min] after the ultrasonic bath, resulting in practically no settling time). The results (Table 2) show clearly that the acid leaching eliminating the fines is the most efficient procedure for reducing the $^{87}\text{Sr}/^{86}\text{Sr}$ value, that is, for removing the secondary phases related to seawater alteration. The indicated procedure (Mahoney, 1987) was applied to samples 12 through 41, and results are reported in Table 3 and Figure 2. The comparison between $^{87}\text{Sr}/^{86}\text{Sr}$ ratios for leached and unleached samples is also shown in Figure 2.

After acid leaching, the remaining powder was rinsed with quartz-distilled water at least 3 times. The final step was centrifugation to separate powder and liquid. The separated powder was dried on a hot plate several times until a constant weight was achieved. The difference between this final weight and the starting weight provides the weight percent loss caused by acid leaching (Table 3). The weight loss reflects, in a large part, the abundance of minerals formed during low-temperature alteration. Unfortunately, no X-ray-diffraction analysis could be done on the remaining powder within the time frame for publication of this manuscript to establish the purity of the material left after acid leaching.

Finally, the sample was processed following standard chemical separation procedures (i.e., HF-HClO₄ dissolution and anion exchange column separation of the different isotopes following the method described in Weis et al., 1987a). The blanks for the columns were less than 3 ng Sr, whereas the total blanks for the whole procedure were less than 6 ng for Sr and less than 2 ng for Nd. These blanks are negligible relative to the concentrations in the samples.

⁵ The 6 N HCl acid is cold, but the solution heats to about 40° in 10 min in the ultrasonic bath.

For Pb isotopes, experience shows that the leaching process does not significantly affect the isotopic ratios (see also Fig. 3) and Sample 121-757C-9R-1, 105–109 cm, which was processed through warm and cold acid leaching shows comparable Pb isotopic ratios within error (see Table 3). In order to speed up the procedure and, most importantly, to reduce the contamination during sample treatment, the samples analyzed for Pb were processed separately without acid leaching in a clean, overpressurized (>3 -mm Hg) laboratory, using reagents purified in a sub-boiling still. Pb was separated on anion exchange columns in an HBr-HCl medium, following a method derived from Manhès et al. (1978). Pb and U concentrations were measured on the same sample solution (aliquants were split before loading on columns and spiked with a ^{235}U - ^{206}Pb mixed spike). U was separated in a HNO₃ medium. Aliquants were taken from these solutions after the first passage on the Pb columns in order to measure the Sr and Nd isotopic compositions of unleached samples.

Sr isotopic composition was measured on double Re filaments with a Finnigan MAT 260 mass spectrometer. The internal precision for the $^{87}\text{Sr}/^{86}\text{Sr}$ ratios is better than 5×10^{-5} . The measured values are normalized to $^{86}\text{Sr}/^{88}\text{Sr} = 0.1194$. Twenty analyses of the NBS 987 Sr standard made during the same time period as the analyses of the ODP samples yielded $^{87}\text{Sr}/^{86}\text{Sr}$ of 0.71022 ± 1 ($2\sigma_m$). An idea of the between-run precision is also given by the replicate analyses reported in Table 3. A few Nd isotopic compositions were measured on double Re filaments with the same Finnigan MAT 260 (13 analyses of the nNd β of Wasserburg et al. [1981] yielded $^{143}\text{Nd}/^{144}\text{Nd} = 0.511910 \pm 13$ and $^{145}\text{Nd}/^{144}\text{Nd} = 0.348436 \pm 11$ [$2\sigma_m$]; for comparison, five analyses of BCR-1 yielded $^{143}\text{Nd}/^{144}\text{Nd} = 0.512682 \pm 47$), but because of the relatively low contents of the leached samples, most of the Nd isotopic compositions were measured on the VG Sector 54 multicollector mass spectrometer (29 analyses of the nNd β yielded $^{143}\text{Nd}/^{144}\text{Nd} = 0.511889 \pm 6$ and $^{145}\text{Nd}/^{144}\text{Nd} = 0.348417 \pm 5$ [$2\sigma_m$]). As most of the Nd isotopic data were obtained on the multicollector mass spectrometer, these latter values for the standard have to be considered for interlaboratory comparison purposes. In both cases, Nd was run as a metal, and for each run the 146, 145, 144, and 143 isotopes were measured with all values normalized to $^{146}\text{Nd}/^{144}\text{Nd} = 0.7219$.

The instrumental neutron activation analysis (INAA) and XRF data precision of the concentration measurements are discussed in Frey et al. (this volume).

Pb isotopic compositions and Pb and U concentrations by the isotope dilution (ID) technique were measured on single Re filaments with a Finnigan MAT 260 mass spectrometer, using the H₃PO₄-silica gel technique (e.g., Cameron et al., 1969). All the results were corrected for mass fractionation ($0.13\% \pm 0.04\%$ per AMU) on the basis of 72 analyses of the NBS 981 Pb standard (Catanzaro et al., 1968) for a temperature range of 1090° to 1200°C. Between-run precision is better than $\approx 0.1\%$ for the $^{206}\text{Pb}/^{204}\text{Pb}$ and $^{207}\text{Pb}/^{204}\text{Pb}$ ratios and better than $\approx 0.15\%$ for the $^{208}\text{Pb}/^{204}\text{Pb}$ ratios. The Pb and U concentrations are given with a precision better than 2%. Total blank values for Pb for the whole chemical procedure were largely less than 1 ng.

ISOTOPIC RESULTS

The isotopic data are reported in Table 3, along with concentrations of Rb-Sr, Sm-Nd, and U-Th-Pb and weight percent loss caused by acid leaching.

Sr and Nd Isotopes

The present-day $^{87}\text{Sr}/^{86}\text{Sr}$ ratios for the leached samples show relatively narrow variations: from 0.70385 to 0.70442 at Site 756, 0.70435 to 0.70560 at Site 757, and 0.70433 to 0.70450 at Site 758. Among the 15 lavas analyzed to date for their Nd isotopic

Table 1. Selected samples for major, trace element, and isotope analyses, Sites 756, 757, and 758.

Core, section, interval (cm)	Unit ^a	Powder isotope chemistry number	Petrographic type ^a	Comments ^b	Color
121-756C-					
10N-1 (Piece 2B, 32-36)	F1	ODP 3	Aphyric basalt		Bluish gray
121-756D-					
4R-1 (Piece 5, 35-39)	F1	ODP 1 (WC-Ag)	Sparsely plagioclase-pyroxene phyric basalt		Brownish gray
4R-1 (Piece 12, 85-89)	F2	ODP 7	Aphyric basalt	Very small empty vesicles	Bluish gray
6R-1 (Piece 2, 6-10)	F4	ODP 8	Altered basalt	Friable due to alteration	Red-brown
6R-2 (Piece 1A, 9-13)	F5	ODP 9	Sparsely plagioclase phyric basalt	Impact of alteration (bluish basalt)	Bluish gray
6R-2 (Piece 1A, 13-17)	F5	ODP 10	Sparsely plagioclase phyric basalt	Compare with previous sample (brown)	Brownish gray
6R-3, 0-8	F5	Ship standard	Sparsely plagioclase phyric basalt		
7R-1 (Piece 12A, 100-104)	F6	ODP 11	Sparsely plagioclase phyric basalt		Bluish, greenish gray
7R-3 (Piece 2C, 50-54)	F6	(+)	Sparsely plagioclase phyric basalt	Impact of alteration (bluish basalt)	Bluish gray
8R-1 (Piece 3, 20-23)	F7	ODP 29	Aphyric basalt	Half the piece (short unit); many vesicles	Reddish brown
9R-2 (Piece 1, 21-24)	F9	+	Aphyric basalt		Bluish gray
10R-1 (Piece 12, 99-103)	F12	ODP 30	Aphyric basalt	Brown staining along small cracks	Bluish gray
10R-3 (Piece 4, 58-63)	F12	+	Aphyric basalt	Native Cu, smectite-filled vesicles	Blue
11R-1 (Piece 16A, 102-106)	F13	+	Aphyric basalt		Dark reddish brown
12R-2, 28-33	F14	Ship standard	Aphyric basalt		
12R-3 (Piece 4F, 139-143)	F14	ODP 25	Aphyric basalt	Vesicles	Bluish gray
121-757C-					
9R-1 (Piece 3, 105-109)	F2	ODP 4/4 bis	Plagioclase-phyric basalt	Few vesicles	Bluish gray, clear
9R-2, 0-10	F2	Ship standard	Plagioclase-phyric basalt		
9R-3 (Piece 1A, 6-10)	F2	+	Plagioclase-phyric basalt	No vesicles	Blue
9R-4 (Piece 1A, 38-42)	F3	+	Plagioclase-phyric basalt	Vesicles, white and light gray fillings	Reddish brown
9R-5 (Piece 1A, 34-38)	F4	ODP 26	Plagioclase-phyric basalt	Less reddish than previous sample, white vesicles	Brown
9R-5 (Piece 2, 70-73)	F5	+	Plagioclase-phyric basalt	Vesicular, top of flow	Brown
9R-6 (Piece 1B, 102-105)	F5	ODP 23	Plagioclase-phyric basalt	Reddish mesostasis, big zeolites, vesicles	Bluish
9R-7 (Piece 1B, 78-82)	F5	ODP 24	Plagioclase-phyric basalt	Contact brown, blue at a veinlet	Mixture, brown-blue
9R-8 (Piece 4A, 54-59)	F5	ODP 13	Plagioclase-phyric basalt	Reddish brown mesostasis, smectites	Brown
10R-1 (Piece 1A, 86-90)	F6	ODP 31	Plagioclase-phyric basalt	Reddish brown mesostasis, few vesicles	Bluish
10R-2 (Piece 5A, 66-70)	F7	+	Highly plagioclase-phyric basalt	Many vesicles, pale grayish mesostasis	Bluish gray
10R-3 (Piece 1, 2-6)	F8	ODP 27	Highly plagioclase-phyric basalt	Many vesicles, blue and white fillings	Pale bluish
10R-3 (Piece 2C, 83-87)	F9	+	Highly plagioclase-phyric basalt	Compare with previous but lighter mesostasis (altered)	Pale bluish
11R-2 (Piece 1, 10-14)	F12	ODP 32	Highly plagioclase-phyric basalt	Dirty green mesostasis, many vesicles	Gray mesostasis
11R-2 (Piece 4, 51-56)	F13	ODP 17	Highly plagioclase-phyric basalt	Many vesicles, blue fillings, green mesostasis	Pale bluish
12R-1 (Piece 2, 100-104)	F18	ODP 2 (WC-Ag)	Moderately plagioclase-phyric basalt	Looks fresher	Dark bluish gray
12R-1 (Piece 2, 104-110)	F18	Ship standard	Moderately plagioclase-phyric basalt		
12R-2 (Piece 1, 0-5)	F18	ODP 14	Moderately plagioclase-phyric basalt	Green mesostasis, no vesicles	Bluish (plagioclase)
12R-4 (Piece 5, 24-29)	F19	ODP 18	Moderately to highly plagioclase-phyric basalt	Very altered, small zeolites, filled vesicles	Reddish brown mesostasis

Core, section, interval (cm)	Unit ^a	Powder isotope chemistry number	Petrographic type ^a	Comments ^b	Color
121-758A-					
54R-2, 70-74	F1	ODP 28	Moderately plagioclase-phyric basalt	Very fine, dark groundmass	
55R-5 (Piece 1D, 82-86)	F1	ODP 33	Moderately plagioclase-phyric basalt	5% plagioclase phenocrystals, coarser grained than next sample—ophitic	
56R-1 (Piece 4A, 64-68)	F1	ODP 34	Moderately plagioclase-phyric basalt	Plagioclase phenocrystals	Greenish gray mesostasis
57R-3 (Piece 2, 18-22)	F2	+	Sparsely plagioclase-phyric basalt	Very fine-grained mesostasis, small plagioclase phenocrystals	Dark dirty green mesostasis
58R-6 (Piece 1C, 21-25)	F2	ODP 5/12	Sparsely plagioclase-phyric basalt		
59R-2 (Piece 1A, 58-62)	F2	ODP 6	Aphyric basalt	Smectites, not too altered	Blue gray
60R-1 (Piece 2B, 122-126)	F3	ODP 35	Aphyric basalt	Much finer grained than next sample	Dark greenish gray
60R-3 (Piece 1A, 18-22)	F3	(+)	Aphyric basalt	Smaller clinopyroxene than next 3 samples, subhedral to euhedral	Mesostasis greenish gray
61R-5 (Piece 1A, 22-26)	F3	+	Aphyric basalt	Fresh, clinopyroxene 1-2 mm	Blue gray (smectites)
62R-1 (Piece 4C, 130-134)	F4	ODP 15	Moderately to highly plagioclase-phyric basalt	Big plagioclase phenocrystals, pervasive smectites	Green dark
62R-3 (Piece 7B, 80-84)	F5	ODP 36	Sparsely plagioclase-phyric basalt	Fine grained	Dirty green
63R-3 (Piece 1, 114-118)	F7	+	Aphyric basalt	Coarse-grained part, fresh, vesicles	Green
65R-1 (Piece 5B, 51-55)	F10	ODP 37	Aphyric basalt	Fine grained	Greenish gray
66R-4, 6-12	F11	Ship standard	Aphyric basalt		Dirty greenish gray
67R-2 (Piece 1B, 92-96)	F13	+	Aphyric basalt	Fine grained	Coarser mottled
67R-4 (Piece 1C, 31-35)	F14	ODP 38	Aphyric basalt	Coarse grained	Mottled gray green
67R-5 (Piece 2B, 86-90)	F15	+	Sparsely plagioclase-phyric basalt	Plagioclase phenocrystals	Mottled bluish green gray
69R-1, 37-43	F17	+	Sparsely plagioclase-phyric basalt		
69R-3 (Piece 1A, 53-57)	F17	ODP 39	Sparsely plagioclase-phyric basalt	Plagioclase phenocrystals, fine grained	
70R-1 (Piece 11A, 71-75)	F18	ODP 19	Aphyric basalt	Small vesicles	Greenish gray
70R-2 (Piece 7F, 129-133)	F19	ODP 20	Aphyric pillow basalt	Fine grained, altered	Dark green gray
71R-1 (Piece 18, 127-131)	F20	ODP 40	Aphyric basalt	Fine grained, small vesicles	Greenish gray
71R-2 (Piece 13, 136-140)	F21	+	Aphyric pillow basalt	Pillow rim, big vesicles	
71R-3 (Piece 3A, 64-68)	F22	ODP 16	Aphyric basalt	Fine grained	Greenish gray
71R-3 (Piece 5D, 140-144)	F23	+	Aphyric basalt	Compare previous sample, some calcite	Greenish gray
72R-2 (Piece 1B, 95-99)	F24	+	Aphyric basalt	Compare with next sample, fine grained	
72R-4 (Piece 1A, 27-31)	F25	+	Aphyric basalt	Fine grained, few vesicles	Greenish
72R-6 (Piece 1, 18-22)	F26	+	Aphyric basalt	Very fine mesostasis	
73R-1 (Piece 7D, 82-86)	F27	ODP 22	Aphyric to sparsely phyric basalt	Plagioclase phenocrystals poor, compare with next sample, small vesicles	
73R-2 (Piece 1A, 10-14)			Aphyric to sparsely phyric basalt	Some plagioclase phenocrystals, fine-grained mesostasis	
73R-3 (Piece 4D, 50-54)	F28	ODP 41	Pillow breccia	Pillow part of the breccia, glassy	
73R-4 (Piece 8, 105-109)	F29	ODP 21	Aphyric basalt	Relatively fine grained	Light gray mottled

^a Defined on board on the basis of macroscopic and thin-section criteria. See Peirce, Weissel, et al. (1989) for a detailed description of the cores.

^b Various observations, including color, that were useful in sample selection.

Table 2. Comparison of acid-leaching procedures for two samples.

Procedure ^a	121-757C-9R-8, 54–59 cm (ODP 13)		121-758A-70R-2, 129–130 cm (ODP 20)	
	⁸⁷ Sr/ ⁸⁶ Sr	Weight loss (%)	⁸⁷ Sr/ ⁸⁶ Sr	Weight loss (%)
Unleached	0.70477 ± 3		0.70474 ± 4	
Cold acid leaching	0.70474 ± 4	21.93	0.70450 ± 2	26.06
Mildly warm acid leaching	0.70480 ± 3	36.74	0.70432 ± 5	37.61
Warm acid leaching	0.70636 ± 3	39.13	0.70514 ± 3	34.93
Mahoney's (1987) leaching	0.70459 ± 4	57.63	0.70432 ± 3	78.61

Note: The isotopic ratios are given with the $2\sigma_m$ (2σ on the mean of the measurement). The weight percent leached is the difference between the powder weight before 6 N HCl acid leaching and the weight of the remaining powder after acid leaching.

^a See text for explanation of the acid-leaching procedures.

composition, present-day ¹⁴³Nd/¹⁴⁴Nd ratios vary between 0.51291 and 0.51285 ($\epsilon_{Nd} = 5.3$ to 4.1) at Site 756, 0.51283 and 0.51276 ($\epsilon_{Nd} = 3.7$ to 2.3) at Site 757, and 0.51291 and 0.51277 ($\epsilon_{Nd} = 5.3$ to 2.5) at Site 758. In an Nd-Sr isotope diagram (Fig. 4), these data plot within the so-called mantle-array, although there is some scatter toward higher ⁸⁷Sr/⁸⁶Sr values, perhaps because all alteration phases were not removed during acid leaching or because these samples were not age corrected. Indeed, no ID concentrations on leached samples are available to allow correction for *in-situ* decay for ⁸⁷Rb and ¹⁴⁷Sm. Assuming a comparable ⁸⁷Rb/⁸⁶Sr range of values for the leached and unleached samples (0 to 0.467), the corresponding maximum corrections for 38, 58, and 88 Ma are, respectively, 0.00025, 0.00038, and 0.00058 for the ⁸⁷Sr/⁸⁶Sr ratios, which is significant; however, these corrections would not remove the variability of the ⁸⁷Sr/⁸⁶Sr ratios. The correction factors are much smaller for Nd because of the longer half-life of ¹⁴⁷Sm in comparison with that of ⁸⁷Rb (1.53×10^{11} yr and 7.04×10^{10} yr). On the other hand, Rb is strongly affected by alteration (Frey et al., this volume), and such corrections are probably meaningless anyway.

Figures 2 and 3 report the weight percent leached vs. different parameters. The purpose of these figures is to show that there is no distinct correlation between alteration degree and Sr isotopic ratios for the leached samples, except for the highest values of the ⁸⁷Sr/⁸⁶Sr ratios. This is especially true at Site 757 (Figs. 2B and 3). The extent of leachable alteration is clearly less in lavas from Site 756 relative to those from the other Leg 121 sites (Figs. 2 and 3), with weight percent loss by leaching varying from 18.4% to 27.7%. Site 756 lavas show no systematic variation of ⁸⁷Sr/⁸⁶Sr vs. depth, although there may be a slight increase in alteration (Fig. 2A). The mean value of 10 leached samples for ⁸⁷Sr/⁸⁶Sr is 0.70399 ± 12 . The Site 757 lavas (Fig. 2B) are much more scattered in ⁸⁷Sr/⁸⁶Sr ratios. They are also more highly altered, which is shown well by the weight percent loss after acid leaching (32.4% to 61.9%), water contents (H₂O⁺ and H₂O⁻), and Fe₂O₃/FeO ratios (see companion paper of Frey et al., this volume). There is no systematic increase of alteration with depth at Site 757. The mean of eight leached samples for ⁸⁷Sr/⁸⁶Sr is 0.70457 ± 9 (excluding Samples 121-757C-10R-3 [Piece 1, 2–6 cm] and 121-757C-11R-2 [Piece 4, 51–56 cm] with distinctly higher ⁸⁷Sr/⁸⁶Sr ratios). Two ⁸⁷Sr/⁸⁶Sr values on Core 121-757C-12R give 0.70446. Site 758 lavas are also relatively altered with weight losses after acid leaching varying from 30.3% to 46.6%. Surprisingly, the ⁸⁷Sr/⁸⁶Sr ratios of leached lavas from Site 758 are very well grouped with a mean value of 18 samples of 0.70438 ± 4 , which is also slightly lower than for lavas from Site 757.

Despite some slight problems related to the effect of alteration on the ⁸⁷Sr/⁸⁶Sr ratios, the three sites appear to have distinct ranges of values. Certainly, most of the Site 756 lavas have distinctly lower ratios than those of the lavas from Sites 757 and 758, which show only partial overlap. Site 757 may have slightly

higher ⁸⁷Sr/⁸⁶Sr values than those of the Site 758 lavas. The Nd-Sr isotope diagram (Fig. 4) well reflects these differences in ⁸⁷Sr/⁸⁶Sr and ¹⁴³Nd/¹⁴⁴Nd ratios among the three Ninetyeast Ridge sites sampled during Leg 121; indeed, Site 758 lavas plot between the Site 756 and Site 757 lavas, and the latter has higher ⁸⁷Sr/⁸⁶Sr and lower ϵ_{Nd} values.

Pb Isotopes

The present-day Pb isotopic ratios at Site 756 vary between 18.672 and 18.817 (relative deviation, $\Delta = 0.78\%$), 15.548 and 15.587 ($\Delta = 0.25\%$), and 38.93 and 39.02 ($\Delta = 0.23\%$) for the ²⁰⁶Pb/²⁰⁴Pb, ²⁰⁷Pb/²⁰⁴Pb, and ²⁰⁸Pb/²⁰⁴Pb ratios, respectively. At Site 757, the corresponding ranges are 18.621 and 19.111 ($\Delta = 2.6\%$) (or 18.901 [$\Delta = 1.5\%$], excluding Sample 121-757C-9R-6 [Piece 1B, 102–105 cm], which has distinctly higher ²⁰⁶Pb/²⁰⁴Pb and ²⁰⁷Pb/²⁰⁴Pb isotopic ratios than any of the other Leg 121 lavas), 15.569 and 15.656 ($\Delta = 0.56\%$) (or 15.617 [$\Delta = 0.31\%$]), and 38.92 and 39.08 ($\Delta = 0.41\%$). At Site 758, the ranges are 18.325 and 18.774 ($\Delta = 2.4\%$), 15.548 and 15.605 ($\Delta = 0.37\%$), and 38.54 and 39.04 ($\Delta = 1.3\%$). These ranges are not significantly changed by a maximum correction⁶ for *in-situ* decay of U and Th for 38 Ma at Site 756, 58 Ma at Site 757, and 88 Ma at Site 758, although the larger spread in (²⁰⁸Pb/²⁰⁴Pb)_i than in measured ratios at all three sites may reflect inaccurate Th data at levels <0.5 ppm (Frey et al., this volume). Nevertheless, despite the error added to the isotopic ratios by the uncertainty of the concentration (2% maximum on the ID determination), each site shows a comparable (²⁰⁶Pb/²⁰⁴Pb)_i and (²⁰⁷Pb/²⁰⁴Pb)_i and a well-grouped range of values (inset of Fig. 5). These are 18.565 to 18.711 ($\Delta = 0.79\%$), 15.545 to 15.583 ($\Delta = 0.24\%$), and 38.46 to 39.02 ($\Delta = 1.5\%$) for the Site 756 basalts; 18.353 to 18.935 ($\Delta = 3.2\%$) (or 18.640 [$\Delta = 1.6\%$], excluding Sample 121-757C-9R-6 [Piece 1B, 102–105 cm]), 15.559 to 15.648 ($\Delta = 0.57\%$) (or 15.604 [$\Delta = 0.29\%$]), and 38.28 to 38.98 ($\Delta = 1.8\%$) (or 38.91 [$\Delta = 1.6\%$]) for the Site 757 basalts; and 18.155 to 18.524 ($\Delta = 2.0\%$), 15.541 to 15.598 ($\Delta = 0.37\%$), and 38.12 to 38.85 ($\Delta = 1.9\%$) for the Site 758 basalts.

On the basis of the initial Pb ratios vs. weight percent loss by acid leaching on the companion aliquants of the same samples (Fig. 3.) as an indication of the degree of leachable alteration of the lavas, it appears that leachable alteration has no consistent major effect on Pb isotopic ratios. Figure 3 also shows the scatter in data for the three Ninetyeast Ridge sites. Site 756 shows the smallest range of Pb isotopic ratios among the three sites. The ²⁰⁶Pb/²⁰⁴Pb and ²⁰⁷Pb/²⁰⁴Pb ratios for Site 758 are closely grouped as well, especially in consideration that the samples represent a much thicker hole: ≈ 180 m of basalts cored, in com-

⁶ Assuming any seawater U was added to the rock soon after eruption (MacDougall, 1977).

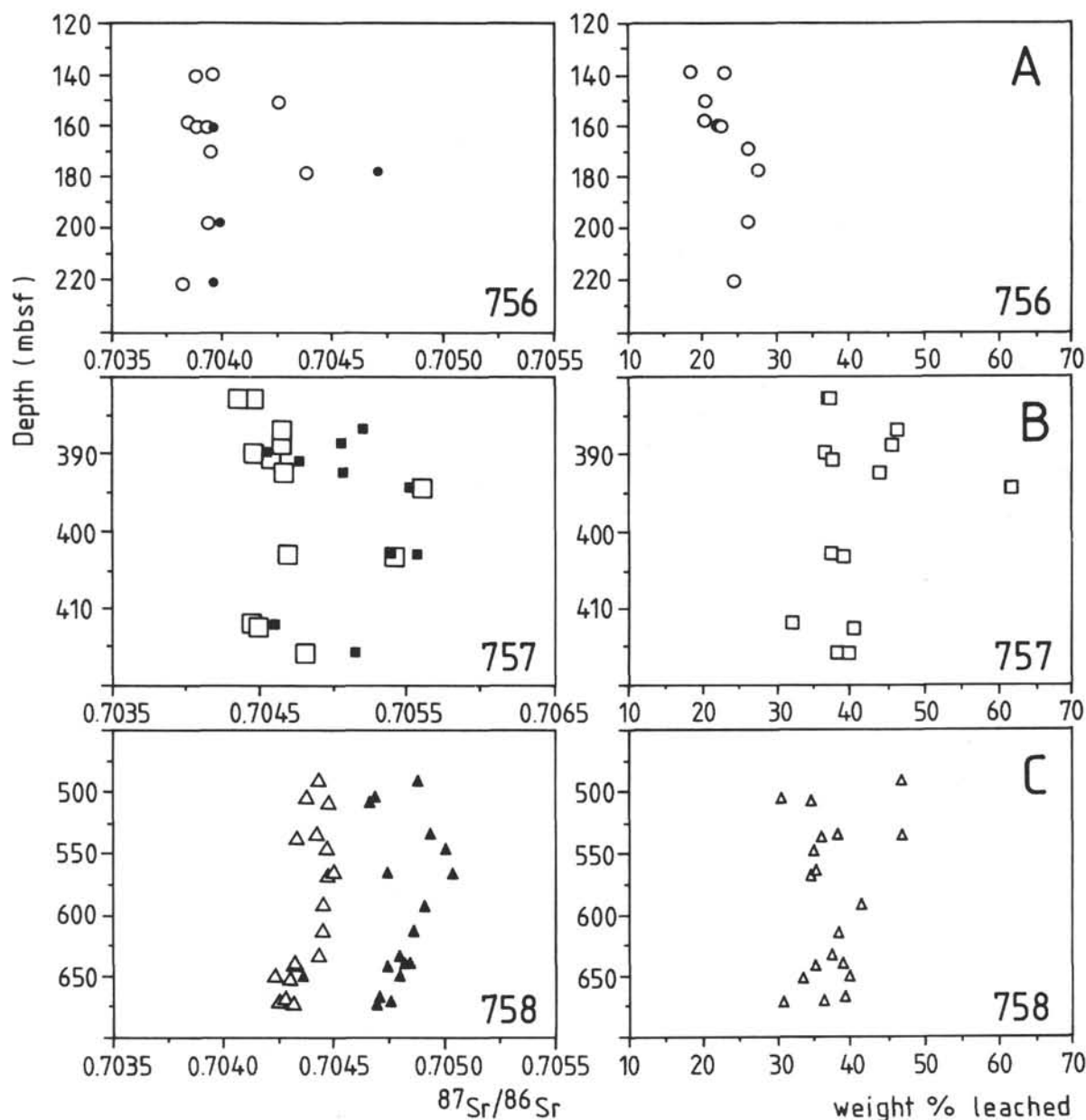


Figure 2. $^{87}\text{Sr}/^{86}\text{Sr}$ of leached samples and weight percent loss by acid leaching (assumed to represent the leachable alteration) vs. depth in m below seafloor (mbsf). The horizontal scales are the same for comparison; the vertical ones differ. The solid symbols correspond to data for unleached samples. A. Site 756. B. Site 757. C. Site 758.

parison with ≈ 80 m at Site 756 and ≈ 35 m at Site 757 (Fig. 6). The Site 757 lavas are much more heterogeneous. This observation is valid even with the exclusion of Sample 121-757C-9R-6 (Piece 1B, 102–105 cm), which has very distinct Pb isotopic ratios that are much more radiogenic than any other values measured on the Ninetyeast Ridge lavas (data from this paper and previous measurements; Dupré and Allègre, 1983; Hart, 1988). According to our shipboard classification, this sample is one of three samples studied for isotopes from flow Unit 757C-F5. If we consider these samples to be from the same flow, then we have an isotopically heterogeneous flow. One has to define the reason for this heterogeneity. Could it be an alteration effect? The sample is described as having a reddish mesostasis and big vesicles filled with zeolites

and geochemically, it is distinctly different with a very high Rb content, the lowest K/Rb, and a high Cs content (Frey et al., this volume), which may reflect the presence of a clay. In the inset of Figure 5, Pb isotopic data for ocean crust vein minerals from DSDP Site 261 (Hart and Staudigel, 1986) are reported to document the effect of alteration on Pb isotopes; clearly, an alteration process similar to the one responsible for the formation of the Site 261 secondary minerals would not account for the distinct Pb isotopic ratios of Sample 121-757C-9R-6 (Piece 1B, 102–105 cm). On the other hand, the possibility that the sample may come from a different flow needs to be checked carefully and will be reconsidered when additional data covering more of Ninetyeast Ridge are available, although the hypothesis would not account

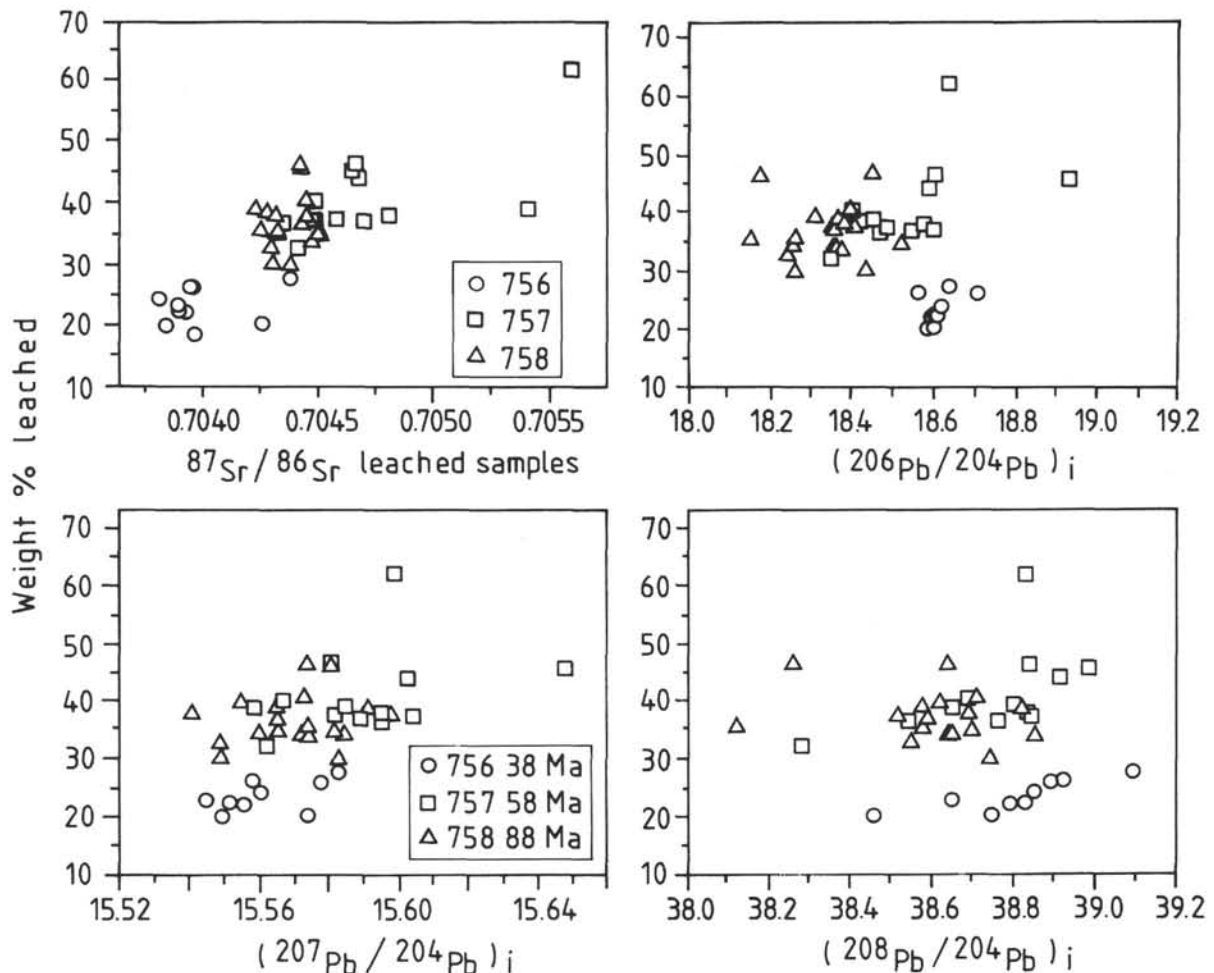


Figure 3. Isotopic ratios ($^{87}\text{Sr}/^{86}\text{Sr}$ of leached samples and age-corrected Pb ratios of unleached samples) vs. weight percent loss by acid leaching on splits analyzed for Sr and Nd isotopic composition. Pb ratios were corrected for *in-situ* U and Th decay by 38 (Site 756), 58 (Site 757), and 88 Ma (Site 758).

for the sample being so out of range in Pb isotopic ratios from all other Site 757 lavas. This sample will not be discussed further in this paper.

Comparison of Figures 6A, 6B, and 6C together with Figure 5 clearly indicates an evolution of the Pb isotopic ratios between the different Ninetyeast Ridge sites: the Pb isotopic ratios become more radiogenic, on average, toward the south (i.e., the Site 756 lavas have more radiogenic Pb ratios than the Site 757 lavas, which have more radiogenic Pb ratios than those at Site 758). This observation is mainly valid for $^{206}\text{Pb}/^{204}\text{Pb}$ and $^{208}\text{Pb}/^{204}\text{Pb}$, as the half-life of ^{235}U is too short to generate any significant variation on these time scales (given the U/Pb ratios of these lavas). It is important to note here that the evolution of the Pb ratios with time would be strengthened if the true age correction could be applied to the individual samples. Indeed, we have no indication, thus far, of the real age of the samples from the bottom of the holes, but, obviously, they are older than the ones from the top, and the real correction for *in-situ* decay of U and Th (and also Rb and Sm) is larger than that applied, which would increase these trends, providing that the measured abundances (in ppm) are the proper ones for correction. On the other hand, the $^{206}\text{Pb}/^{204}\text{Pb}$ correction is almost certainly a maximum because U has probably increased in most of the rocks with progressive alteration (MacDougall, 1977).

The three samples from Core 121-757C-12R that are very distinctive in major and trace element contents (see companion paper of Frey et al., this volume) also have slightly distinct Pb isotopic ratios relative to the rest of the Hole 757C lavas, with less radiogenic values calculated at 58 Ma (Fig. 6): $(^{206}\text{Pb}/^{204}\text{Pb})_i = 18.353\text{--}18.419$, $(^{207}\text{Pb}/^{204}\text{Pb})_i = 15.559\text{--}15.567$, and $(^{208}\text{Pb}/^{204}\text{Pb})_i = 38.28\text{--}38.69$. They are also more enriched in large-ion lithophile elements and have higher Th and U contents (Table 3).

DISCUSSION: COMPARISON WITH THE KERGUELEN-HEARD HOT SPOT AND OTHER INDIAN OCEAN FEATURES

The isotopic measurements confirm previous inferences based on shipboard major and trace element XRF analyses (Leg 121 Scientific Party, 1988; Leg 121 Shipboard Scientific Party, 1988; Weis et al., in press) and previous work on DSDP samples from Ninetyeast Ridge (Frey et al., 1977). The Ninetyeast Ridge lavas are tholeiitic basalts, but compositionally and isotopically they are not similar to MORBs but are similar to OIBs. Indeed, in the Nd-Sr isotope diagram (Fig. 4), several of the Ninetyeast Ridge lavas plot in the upper left-hand field, with slightly positive ϵ_{Nd} values, between the Foch Island tholeiites (White and Hofmann, 1982; W. M. White, pers. comm., 1985) and the transitional basalts (Gautier et al., in press) of the Kerguelen Archipelago. The

Site 756 data also plot close to the two data points obtained for lavas from St. Paul Island (Michard et al., 1986; Dosso et al., 1988), which is located near the Southeast Indian Ridge axis. The Leg 121 data points lie in a position intermediate between data for Indian Ocean spreading-ridge basalts (Le Roex et al., 1983; Hamelin and Allègre, 1985; Hamelin et al., 1985/1986; Michard et al., 1986; Price et al., 1986; Dosso et al., 1988) and a very enriched OIB-type component (i.e., very low ϵ_{Nd} and high $^{87}Sr/^{86}Sr$ values), with characteristics entirely comparable to the most differentiated lavas from the Kerguelen Archipelago (D. Weis, unpubl. data).

The isotopic evolution of the Kerguelen Archipelago basalts ranges from slightly depleted values ($\epsilon_{Nd} \leq 0$ and $^{87}Sr/^{86}Sr < 0.705$) in the 40- to 26-Ma-old transitional basalts to more enriched values ($\epsilon_{Nd} < 0$ and $^{87}Sr/^{86}Sr > 0.705$) in the younger, 26- to 0-Ma-old highly alkaline series and differentiated lavas (Nougier et al., 1983; Gautier et al., 1989). A model developed to account for this geochemical evolution (Weis et al., 1989b; Gautier et al., in press) invokes mixing between two mantle components: a depleted, high- ϵ_{Nd} MORB component, like that erupted today on the Southeast Indian Ridge (e.g., Dosso et al., 1988), and a very enriched, low- ϵ_{Nd} component that is represented by the young differentiated lavas present on the Kerguelen Archipelago, the phonolites and phonolitic tephrites of the southeast province (Gautier et al., 1989). The relative proportions of these two end members have evolved with time, reflecting the tectonic setting of the archipelago. When the islands first formed, ≈ 40 Ma ago (Nougier et al., 1983), they were above or close to the spreading-ridge axis. Therefore, the MORB component had greater importance in the mixing, which led to tholeiitic-transitional magmatism. As the spreading axis migrated away from the islands, the influence of the MORB component decreased, until finally disappearing in the young, most differentiated lavas, which reflect dominantly the Kerguelen hot spot. In this model, the Foch Island tholeiites represent an early stage of the Kerguelen Archipelago evolution. Their eruption was followed very quickly by those of the transitional magmatism. In the Nd-Sr isotope diagram (Fig. 4), the position of most of the Ninetyeast Ridge lavas is intermediate between those of the Foch Island tholeiites and the transitional basalts. Thus, the isotopic data are consistent with a mixing model between a depleted MORB-type component and a very enriched OIB-type component, as also suggested on the basis of the trace element characteristics of the Leg 121 lavas (Leg 121 Scientific Party, 1988; Weis et al., in press).

The question now is how to use the Leg 121 lavas to define with greater precision the different components that have been involved in the mixing process and how the relative mixing proportions have varied with time.

Our interpretations mainly emphasize Pb isotopic data because these data are available for the whole sample series of Leg 121. In addition, Pb isotopes are a good tracer of the Dupal anomaly.

In Figure 5, the Pb isotopic data for the Ninetyeast Ridge lavas are compared with data obtained thus far for samples from the Kerguelen Archipelago. The data range for the Kerguelen samples is relatively large and is entirely overlapped by data for the Heard volcanic rocks (Barling et al., 1988; Storey et al., 1988; S. L. Goldstein, pers. comm., 1989). Data for the lavas from the southeast province of the Kerguelen Archipelago (D. Weis, unpubl. data) show an isotopic evolution from basalts and trachytes, which have Pb, Sr, and Nd isotopic ratios overlapping those of the mildly alkaline basalts *sensu stricto* ($^{87}Sr/^{86}Sr \approx 0.705$ and $\epsilon_{Nd} \leq 0$) of the archipelago, toward the distinctly more enriched values for the phonolites and tephritic phonolites, with $^{87}Sr/^{86}Sr$ up to 0.708 and ϵ_{Nd} down to -3 . Contrary to the basaltic series, which have nearly uniform Pb isotopic ratios (Weis et al., 1989a, 1989b), these southeast province volcanic rocks show an evolution in their

Pb isotopic ratios. Specifically, the phonolites and phonolitic tephrites have distinctly less radiogenic $^{206}Pb/^{204}Pb$ and, to a lesser extent, $^{208}Pb/^{204}Pb$ ratios than the basalts (Fig. 5). In Figure 7, especially for $^{208}Pb/^{204}Pb$ vs. $^{206}Pb/^{204}Pb$ (Fig. 7B), these young differentiated Kerguelen samples plot distinctly to the left of the trend defined by the Indian Ocean MORBs and other Indian OIBs. This geochemical trend is also temporal, as the basalts and trachytes are 23–25 Ma old whereas the most differentiated lavas are 6–10 Ma old. The five dredged basalts from the Kerguelen Plateau, although entirely similar in their range of Nd-Sr isotopic values (Davies et al., 1989; Weis et al., 1989a), extend the Archipelago values toward less radiogenic Pb ratios, as confirmed by the recent measurement of Leg 120 basalts (V. Salters, pers. comm., 1989). The compositions of the late differentiated lavas, which are the most extreme in Sr and Nd isotopic values and with even stronger Dupal anomaly characteristics in their Pb ratios (i.e., higher $^{207}Pb/^{204}Pb$ and $^{208}Pb/^{204}Pb$ for a given $^{206}Pb/^{204}Pb$ ratio in comparison with the Northern Hemisphere reference line [NHRL] of Hart [1984]), can be considered as the purest representatives of those of the Kerguelen hot spot, without any detectable depleted-component influence.

In a Pb-Pb diagram (Figs. 5 and 7), the age-corrected Ninetyeast Ridge data plot within the field for the Kerguelen Archipelago and show a smaller range of variation. Thus, like the Kerguelen Archipelago, the Ninetyeast Ridge lavas have a typical Dupal anomaly signature (Dupré and Allègre, 1983; Hart, 1984). In more detail, the Site 758 lavas have Pb isotopic ratios intermediate between those of the pure Kerguelen hot spot and the Foch Island tholeiites. In contrast, the Site 756 lavas are at the limit of the Kerguelen Archipelago field—not the hot-spot field per se—with slightly more radiogenic $^{206}Pb/^{204}Pb$ values, pointing toward the radiogenic extremity of the Indian Ocean MORB trend, to the field defined by lavas from St. Paul Island (Fig. 7). This is even more striking in a $^{87}Sr/^{86}Sr$ vs. $^{206}Pb/^{204}Pb$ diagram (Fig. 8A), where the Kerguelen data field shows a broad negative trend (with a -1 slope) extending from the field defined by the late differentiated lavas (i.e., the Kerguelen hot spot per se) to the few data points obtained for St. Paul Island (Dupré and Allègre, 1983; Michard et al., 1986; Dosso et al., 1988) and, to a lesser extent, Amsterdam Island (Dupré and Allègre, 1983; Hamelin et al., 1985/1986). Interestingly, the basalts from the Kerguelen Plateau (dredged samples of Weis et al., 1989a; Leg 120 samples of V. Salters, pers. comm., 1989) follow the same trend although they extend it toward much lower $^{206}Pb/^{204}Pb$ values. Comparable observations can be made in a $^{143}Nd/^{144}Nd$ vs. $^{206}Pb/^{204}Pb$ diagram (Fig. 8B), considering in this case that the Kerguelen Archipelago data field shows a broad positive trend. In both Figures 8A and 8B, excepting the Site 757 lavas with high $^{87}Sr/^{86}Sr$ ratios, the Ninetyeast Ridge lavas, including the little previously published data for the DSDP samples (Dupré and Allègre, 1983), follow the same trend. More specifically, data for the lavas from Sites 757 and 758 plot within the Kerguelen Archipelago field whereas those for the Site 756 lavas extend the field toward lower $^{87}Sr/^{86}Sr$ and higher $^{143}Nd/^{144}Nd$ values and plot near the field of St. Paul Island.

Trace element vs. isotopic ratio diagrams show comparable types of relationships, although the correlation between isotopic ratios and an incompatible element ratio, such as $(La/Sm)_n$, is complex. In a $(La/Sm)_n$ vs. $^{87}Sr/^{86}Sr$ diagram (Fig. 9A), the Ninetyeast Ridge lavas with the lowest $^{87}Sr/^{86}Sr$ ratios plot on what can be interpreted as a mixing hyperbola between the Southeast Indian Ridge basalts (Dosso et al., 1988) and the Kerguelen hot spot, at the same $(La/Sm)_n$ level as the St. Paul Island lavas. However, in detail (as in Fig. 8), the lavas from Site 756 generally are close to the field of the St. Paul lavas and similar source components can be inferred. In a $(La/Sm)_n$ vs. $^{206}Pb/^{204}Pb$ dia-

Table 3. Sr, Pb, and Nd isotopic compositions and Rb, Sr, Nd, Sm, U, Th, and Pb concentrations for the Ninetyeast Ridge lavas from Sites 756, 757, and 758.

Core, section, interval (cm)	Unit	Petrographic type	Chemistry number	Rb (ppm)	Sr (ppm)	$^{87}\text{Rb}/$ ^{86}Sr	$^{87}\text{Sr}/^{86}\text{Sr}$		Weight percent (leached)	(leached)
							(unleached)	$2\sigma_m$		
121-756C-										
10N-1, 32-36	F1	Aphyric basalt	ODP 3	6.5	188				20.36	0.70426
121-756D-										
4R-1, 35-39	F1	Sparsely plagioclase-pyroxene phyric basalt	ODP 1	10	195				18.44	0.70396
4R-1, 85-89	F2	Aphyric basalt	ODP 7	15	181				23.10	0.70389
6R-1, 6-10	F4	Altered basalt	ODP 8	19	166				20.33	0.70385
6R-2, 9-13	F5	Sparsely plagioclase phyric basalt	ODP 9	33	171	0.5584	0.70396	3	22.30	0.70393
									18.64	
6R-2, 13-17	F5	Sparsely plagioclase phyric basalt	ODP 10	1.1	174				22.53	0.70389
7R-1, 100-104	F6	Sparsely plagioclase phyric basalt	ODP 11	2.9	200				26.30	0.70395
8R-1, 20-23	F7	Aphyric basalt	ODP 29	13	153	0.2459	0.70470	2	27.68	0.70438
									0.70440	
									0.70442	
10R-1, 99-103	F12	Aphyric basalt	ODP 30	16	156	0.2968	0.70399	1	26.35	0.70394
12R-3, 139-143	F14	Aphyric basalt	ODP 25	1.9	163	0.0337	0.70396	1	24.29	0.70382
121-757C-										
9R-1, 105-109	F2	Plagioclase-phyric basalt	ODP 4	1.4	176				36.84	0.70435
	F2	Plagioclase-phyric basalt	ODP 4"	1.4	176				37.20	0.70446
9R-5, 34-38	F4	Plagioclase-phyric basalt	ODP 26	11	313	0.1017	0.70520	3	46.37	0.70466
9R-6, 102-105	F5	Plagioclase-phyric basalt	ODP 23	35	215	0.4711	0.70505	3	45.69	0.70465
							0.70506	4		
9R-7, 78-82	F5	Plagioclase-phyric basalt	ODP 24	18	181	0.2878	0.70457	2	36.71	0.70447
9R-8, 54-59	F5	Plagioclase-phyric basalt	ODP 13	22	184	0.346	0.70477	3	37.75	0.70459
10R-1, 86-90	F6	Plagioclase-phyric basalt	ODP 31	17	247	0.1992	0.70508	1	44.05	0.70467
10R-3, 2-6	F8	Highly plagioclase-phyric basalt	ODP 27	17	559	0.088	0.70552	3	61.91	0.70560
11R-2, 10-14	F12	Highly plagioclase-phyric basalt	ODP 32	19	324	0.1697	0.70540	2	37.42	0.70469
11R-2, 51-56	F13	Highly plagioclase-phyric basalt	ODP 17	20	292	0.1982	0.70557	4	39.13	0.70541
12R-1, 100-104	F18	Moderately plagioclase-phyric basalt	ODP 2	7.8	164				32.37	0.70443
12R-2, 0-5	F18	Moderately plagioclase-phyric basalt	ODP 14	20	160	0.3617	0.70460	5	40.37	0.70449
12R-4, 24-29	F19	Moderately to highly plagioclase-phyric	ODP 18	14	150	0.2701	0.70514	5	38.50	0.70481
							0.70515	3	39.84	
121-758A-										
54R-2, 73-76	F1	Moderately plagioclase-phyric basalt	ODP 28	0.9	148	0.0176	0.70488	3	46.59	0.70443
55R-5, 82-86	F1	Moderately plagioclase-phyric basalt	ODP 33	0.4	122	0.0095	0.70469	2	30.33	0.70438
56R-1, 64-68	F1	Moderately plagioclase-phyric basalt	ODP 34	1.4	127	0.0319	0.70467	3	34.47	0.70448
58R-6, 21-25	F2	Sparsely plagioclase phyric basalt	ODP 5	1.1	143				46.63	0.70442
58R-6, 21-25	F2	Sparsely plagioclase phyric basalt	ODP 12	1.1	143	0.0223	0.70493	3	38.02	
59R-2, 58-62	F2	Aphyric basalt	ODP 6	2.2	127				35.90	0.70433
60R-1, 122-126	F3	Aphyric basalt	ODP 35	0.6	131	0.0133	0.70500	3	34.70	0.70447
62R-1, 130-134	F4	Moderately to highly plagioclase-phyric	ODP 15	0.9	139	0.0187	0.70474	3	35.06	0.70450
62R-3, 80-84	F5	Sparsely plagioclase phyric basalt	ODP 36	0.7	157	0.0129	0.70503	2	34.55	0.70447
65R-1, 51-55	F10	Aphyric basalt	ODP 37	0.4	157	0.0074	0.70491	2	41.10	0.70443
67R-4, 31-35	F14	Aphyric basalt	ODP 38	0.2	144	0.004	0.70486	2	38.33	0.70445
69R-3, 53-57	F17	Sparsely plagioclase phyric basalt	ODP 39	0.7	114	0.0178	0.70479	3	37.35	0.70443
70R-1, 71-75	F18	Aphyric basalt	ODP 19	0.1	140	0.0021	0.70482	2	38.87	0.70432
							0.70484	2		
70R-2, 129-130	F19	Aphyric pillow basalt	ODP 20	0.5	125	0.0116	0.70474	4	34.93	0.70432
71R-1, 127-131	F20	Aphyric basalt	ODP 40	0.8	130	0.0178	0.70479	^a 6	39.67	0.70423
							0.70481	3		
71R-3, 64-68	F22	Aphyric basalt	ODP 16	0.1	122	0.0024	0.70436	4	33.24	0.70430
73R-1, 82-86	F27	Aphyric to sparsely plagioclase-phyric	ODP 22	0	121	0	0.70470	3	39.00	0.70428
73R-3, 50-54	F28	Pillow breccia	ODP 41	0.4	115	0.0101	0.70475	^a 8	36.00	0.70425
							0.0101	2		
73R-4, 105-109	F29	Aphyric basalt	ODP 21	1.5	113	0.0384	0.70469	2	30.68	0.70431

gram (Fig. 9B), data from Site 757 lie between those for the Kerguelen Archipelago transitional basalts and St. Paul Island lavas, and the results from Site 758 lie between those from the Southeast Indian Ridge and St. Paul Island, but in the $(\text{La}/\text{Sm})_n$ vs. $^{87}\text{Sr}/^{86}\text{Sr}$ diagram (Fig. 9A), they extend to high $^{87}\text{Sr}/^{86}\text{Sr}$ values, distinctly beyond the trend connecting the Southeast Indian Ridge and St. Paul fields. In fact, as discussed by Frey et al.

(this volume), the lavas from Sites 757 and 758 have distinctly different incompatible trace element contents and ratios, which accounts for these sites not forming a single continuous mixing trend in La/Sm vs. isotopic ratios plots.

On the basis of the data we have thus far, the Site 756 lavas could have a comparable mode of formation to those of St. Paul Island. They result from mixing between a MORB component, the

Table 3 (continued).

$^{87}\text{Sr}/^{86}\text{Sr}$ $2\sigma_m$	Sm (ppm)	Nd (ppm)	$^{143}\text{Nd}/^{144}\text{Nd}$ $2\sigma_m$		ϵ_{Nd}	Pb (ppm)	U (ppm)	Th (ppm)	$^{206}\text{Pb}/^{204}\text{Pb}$	$^{207}\text{Pb}/^{204}\text{Pb}$	$^{208}\text{Pb}/^{204}\text{Pb}$	$^{87}\text{Sr}/^{86}\text{Sr}$ (initial)
Site 756—38 Ma												
3	4.7	17.1	0.51291	2	5.3	0.59	0.10	1.26	18.672	15.577	39.02	
2	4.8	16.4						1.17	18.705	15.548	38.93	
3	5.1	16.8				0.56	0.10	1.33	18.682	15.548	38.95	
1	5.4	18.7				0.40	0.08	1.7	18.673	15.553	38.99	
5	4.0	12.9				0.41	0.09	0.71	18.696	15.560	39.04	0.70366
2	4.2	14.0				0.37	0.09	0.7	18.710	15.556	39.03	
1	4.7	16.8	0.51291	3	5.3	0.80	0.38	1.01	18.745	15.567	39.05	
2	3.9	14.6				0.93	0.22	0.88	18.735	15.587	39.21	0.70457
4												
4												
3	3.8	13.5				0.86	0.24	0.66	18.817	15.583	39.02	0.70383
2	4.2	13.4	0.51285	3	4.1	0.79	0.17	0.68	18.702	15.565	38.96	0.70394
Site 757—58 Ma												
6	1.6	5.7	0.51282	6	3.6	0.14	0.04	0.33	18.717	15.598	38.99	
4						0.15	0.07		18.738	15.617	39.03	
2	1.4	5.2				0.37	0.13	0.24	18.809	15.592	38.96	0.70512
2	1.7	4.6				0.53	0.16	0.28	19.111	15.656	39.08	0.70466
2	1.5	5.3	^b 0.51279	3	2.9	0.38	0.15	0.43	18.828	15.606	38.98	0.70433
4	1.4	5.1	^b 0.51279	4	2.9	0.34	0.11	0.24	18.767	15.604	38.96	0.70448
3	1.1	4.0				0.28	0.11	0.09	18.820	15.614	38.97	0.70492
2	1.6	5.9				0.29	0.13	0.25	18.901	15.611	39.00	0.70545
3	1.8	6.1	0.51281	2	3.3	0.49	0.19	0.35	18.715	15.593	38.98	0.70526
4	1.7	6.0				0.46	0.18	0.34	18.684	15.596	38.94	0.70541
2	3.8	14.4				0.37	0.30	1.53	18.825	15.584	39.07	
1	3.7	14.3				0.79	0.45	1.48	18.732	15.583	39.05	0.70430
2	1.3	16.0	0.51276	1	2.3	1.35	0.47	1.89	18.621	15.569	38.92	0.70492
			^b 0.51283	3	3.7							
Site 758—88 Ma												
3	2.1	6.3	^b 0.51288	3	4.8	0.55	0.11	0.28	18.627	15.582	38.79	0.70486
1	1.8	4.7				0.13	0.07		18.738	15.572	38.89	0.70468
3	2.1	5.0	^b 0.51289	1	4.9	0.21	0.08		18.707	15.590	38.84	0.70463
2	4.2	14.2	0.51291	3	5.3	0.53	0.09	0.73	18.325	15.588	38.65	
	4.2	14.2	0.51282	1	3.5	0.97	0.17	0.73	18.564	15.605	38.74	0.70490
			^b 0.51284	4	4.0							
5	2.4	7.6				0.20	0.04	0.29	18.329	15.573	38.54	
3	2.6	9.0				0.32	0.14	0.43	18.752	15.578	39.04	0.70498
4	1.7	5.5				0.56	0.08	0.23	18.650	15.588	38.82	0.70472
4	3.4	10.9				0.51	0.20	0.27	18.729	15.602	39.00	0.70501
5	2.6	9.0				0.30	0.12	0.33	18.749	15.590	39.03	0.70490
3	2.7	10.4	^b 0.51287	1	4.4	0.75	0.13	0.19	18.505	15.548	38.76	0.70485
3	2.4	8.3				0.21	0.10	0.28	18.774	15.585	38.98	0.70477
4	2.3	8.3				0.41	0.12	0.22	18.622	15.603	38.98	0.70482
								0.22	18.629	15.588	38.95	
3	2.2	7.8	0.51277	5	2.5	0.33	0.12	0.25	18.576	15.588	38.87	0.70473
4	2.1	7.9				0.30	0.11	0.27	18.635	15.570	38.88	0.70477
2	2.3	7.3				0.37	0.11	0.33	18.504	15.561	38.81	0.70436
3	2.3	7.0	0.51283	1	3.8	0.43	0.11	0.41	18.606	15.576	38.85	0.70470
			^b 0.51285	1	4.2							
2	2.4	8.8				0.34	0.11	0.35	18.547	15.588	38.88	0.70474
												0.70482
1	2.5	8.3				1.46	0.11	0.26	18.503	15.586	38.79	0.70464

Kerguelen hot spot, although in a distinctly lower proportion than for the lavas at Sites 757 and 758, and another Indian Ocean mantle source, which could be another plume, a St. Paul (or Amsterdam) plume. Clearly, two-component mixing is not satisfactory to account for the variations observed in the Ninetyeast Ridge lavas, which is not too surprising in view of the relatively complicated setting in which they were generated.

NINETYEAST RIDGE ORIGIN AND THE DUPAL ANOMALY

The isotopic data presented in this paper indicate that the Ninetyeast Ridge lavas derive from mixing between at least three components: a depleted MORB-like component, a Kerguelen hot spot-type component, and a component comparable to that sam-

Table 3 (continued).

Core, section, interval (cm)	$(^{206}\text{Pb}/^{204}\text{Pb})_i$	$(^{207}\text{Pb}/^{204}\text{Pb})_i$	$(^{208}\text{Pb}/^{204}\text{Pb})_i$	$^{238}\text{U}/^{204}\text{Pb}$	$^{235}\text{U}/^{204}\text{Pb}$	$^{232}\text{Th}/^{204}\text{Pb}$	Th/U
121-756C-							
10N-1, 32-36	18.608	15.574	38.75	10.88	0.0789	141.64	12.60
121-756D-							
4R-1, 35-39							
4R-1, 85-89	18.614	15.545	38.65	11.45	0.0830	157.32	13.30
6R-1, 6-10	18.597	15.550	38.46	12.83	0.0930	281.66	21.25
6R-2, 9-13	18.613	15.556	38.83	14.09	0.1022	114.90	7.89
6R-2, 13-17	18.618	15.552	38.79	15.62	0.1133	125.52	7.78
7R-1, 100-104	18.565	15.559	38.89	30.52	0.2214	83.83	2.66
8R-1, 20-23	18.645	15.583	39.09	15.24	0.1105	62.98	4.00
10R-1, 99-103	18.711	15.578	38.92	17.95	0.1302	51.00	2.75
12R-3, 139-143	18.620	15.561	38.85	13.80	0.1001	57.06	4.00
121-757C-							
9R-1, 105-109	18.551	15.590	38.54	18.35	0.1331	156.40	8.25
	18.467	15.604		30.00	0.2176		
9R-5, 34-38	18.605	15.582	38.84	22.58	0.1638	43.07	1.85
9R-6, 102-105	18.935	15.648	38.98	19.53	0.1416	35.31	1.75
9R-7, 78-82	18.599	15.595	38.76	25.39	0.1841	75.20	2.87
9R-8, 54-59	18.579	15.595	38.83	20.78	0.1507	46.85	2.18
10R-1, 86-90	18.592	15.603	38.91	25.26	0.1832	21.36	0.82
10R-3, 2-6	18.640	15.599	38.83	28.86	0.2093	57.36	1.92
11R-2, 10-14	18.490	15.582	38.84	24.89	0.1805	47.38	1.84
11R-2, 51-56	18.457	15.585	38.80	25.10	0.1820	48.99	1.89
12R-1, 100-104	18.353	15.562	38.28	52.19	0.3785	275.03	5.10
12R-2, 0-5	18.401	15.567	38.69	36.61	0.2655	124.41	3.29
12R-4, 24-29	18.419	15.559	38.65	22.30	0.1617	92.65	4.02
121-758A-							
54R-2, 73-76	18.451	15.574	38.64	12.79	0.0928	33.64	2.55
55R-5, 82-86	18.263	15.549		34.53	0.2504		
56R-1, 64-68	18.372	15.574		24.41	0.1770		
58R-6, 21-25	18.177	15.581	38.26	10.80	0.0783	90.49	8.11
58R-6, 21-25	18.410	15.598	38.52	11.19	0.0812	49.67	4.29
59R-2, 58-62	18.155	15.565	38.12	12.69	0.0921	95.09	7.25
60R-1, 122-126	18.366	15.560	38.65	28.12	0.2039	89.24	3.07
62R-1, 130-134	18.524	15.582	38.70	9.14	0.0663	27.16	2.88
62R-3, 80-84	18.383	15.585	38.85	25.19	0.1827	35.14	1.35
65R-1, 51-55	18.396	15.573	38.71	25.71	0.1865	73.05	2.75
67R-4, 31-35	18.353	15.541	38.69	11.06	0.0802	16.70	1.46
69R-3, 53-57	18.354	15.565	38.59	30.59	0.2219	88.51	2.80
70R-1, 71-75	18.364	15.591	38.82	18.77	0.1361	35.56	1.83
70R-2, 129-130	18.256	15.573	38.65	23.27	0.1687	50.08	2.08
71R-1, 127-131	18.312	15.555	38.62	23.48	0.1703	59.54	2.45
71R-3, 64-68	18.243	15.549	38.55	18.98	0.1377	58.84	3.00
73R-1, 82-86	18.381	15.565	38.58	16.37	0.1187	63.04	3.73
73R-3, 50-54	18.263	15.574	38.58	20.69	0.1501	68.04	3.18
73R-4, 105-109	18.437	15.583	38.74	4.81	0.0349	11.75	2.36

Note: Rb, Sr: XRF; Sm, Th: INAA; Pb, U: ID. The weight percent leached is the difference between the weight of the powder before 6 N HCl acid leaching and that of the remaining powder after acid leaching. For Sr and Nd isotopic composition, the measured ratios are given with the $2\sigma_m$ (2σ on the mean of the measurement), whereas for Pb, the 2σ precision is $<0.1\%$ for $^{206}\text{Pb}/^{204}\text{Pb}$ and $^{207}\text{Pb}/^{204}\text{Pb}$ and $<0.15\%$ for $^{208}\text{Pb}/^{204}\text{Pb}$. Measured ratios are normalized to $^{86}\text{Sr}/^{88}\text{Sr} = 0.1194$ for Sr isotopic ratios and to $^{146}\text{Nd}/^{144}\text{Nd} = 0.7219$ for Nd isotopic ratios. For Pb, a mass-fractionation correction factor of $0.13\% \pm 0.04\%$ per atomic mass unit was applied to all the isotopic ratios, on the basis of 72 analyses of the NBS 981 Pb standard. The "initial" ratios were calculated at 38 Ma for Site 756, 58 Ma for Site 757, and 88 Ma for Site 758 (Peirce, Weissel, et al., 1989; R. A. Duncan, pers. comm., 1990). "Initial" $^{87}\text{Sr}/^{86}\text{Sr}$ ratios were calculated for unleached samples on the basis of their XRF-measured Rb and Sr concentrations. Assuming a comparable $^{87}\text{Rb}/^{86}\text{Sr}$ range (0 to 0.467) in the acid-leached samples to that in the unleached samples, the corresponding maximum corrections for 38, 58, and 88 Ma are, respectively, 0.00025, 0.00038, and 0.00058 for the $^{87}\text{Sr}/^{86}\text{Sr}$ ratios, which is significant, but will not change the general interpretation of the origin of Ninetyeast Ridge. The correction factors are much smaller for Nd because of the longer half-life of ^{147}Sm in comparison with ^{87}Rb (1.53×10^{11} and 7.04×10^{10} yr).

^a Within-run precision was not satisfactory, and a second analysis was performed on the mass spectrometer.

^b Analyses performed on acid-leached samples.

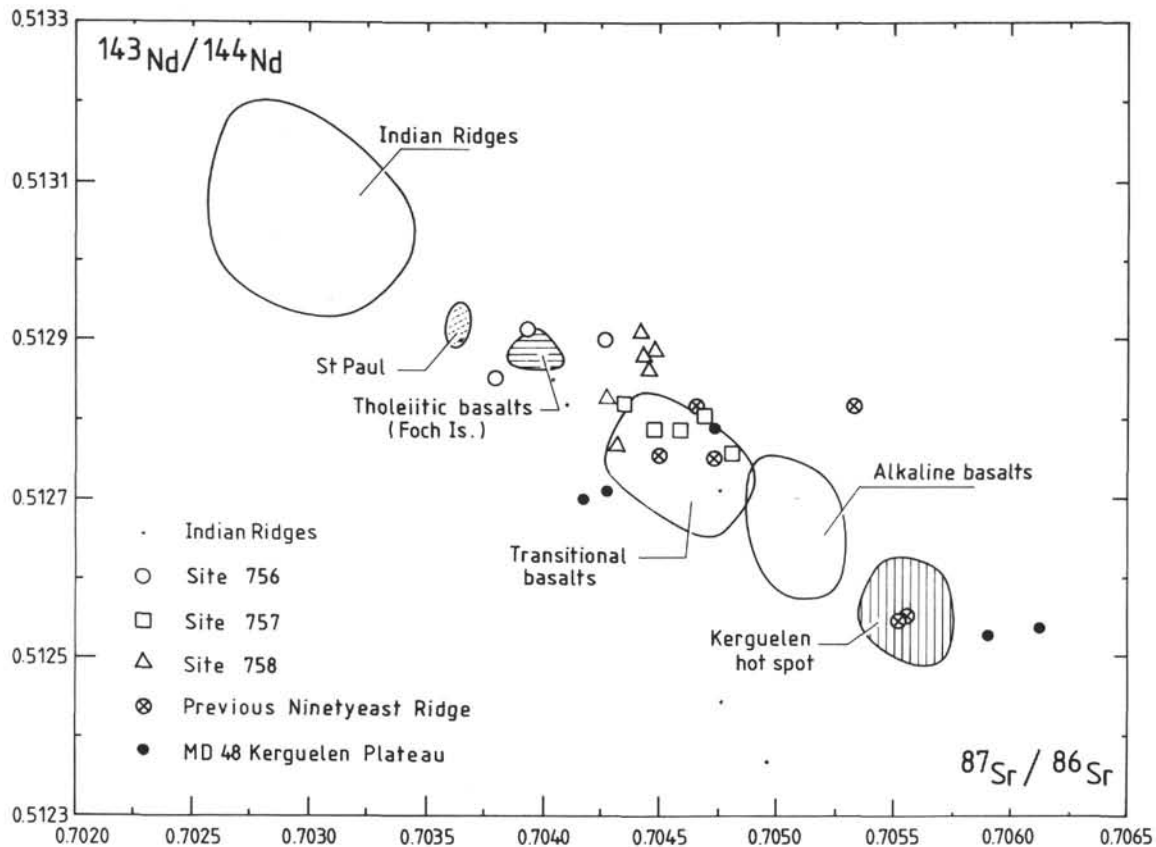


Figure 4. $^{143}\text{Nd}/^{144}\text{Nd}$ vs. $^{87}\text{Sr}/^{86}\text{Sr}$ diagram comparing present-day data for Leg 121 lavas (previous DSDP sites on Ninetyeast Ridge: Mahoney et al., 1983), Indian Ocean ridges (Indian Ocean triple junction: Price et al., 1986; Rodriguez: Michard et al., 1986; Southwest Indian Ridge: Le Roex et al., 1983, 1985; Hamelin and Allègre, 1985; SEIR [Southeast Indian Ridge]: Dosso et al., 1988; East Indian Ridge: Hamelin et al., 1985/1986), St. Paul Island (Michard et al., 1986; Dosso et al., 1988), Kerguelen Archipelago (Foch Island: White and Hofmann, 1982; transitional, mildly alkaline and highly alkaline basalts [= Kerguelen hot spot]: Weis et al., 1989b; Gautier et al., in press), and Kerguelen Plateau (MD48: Weis et al., 1989a).

pled by the St. Paul (and Amsterdam) lavas. The depleted component is comparable to that sampled by basalts from the north part of the Southeast Indian Ridge, between the Indian Ocean triple junction and the islands of St. Paul and Amsterdam. The Kerguelen-type, very enriched component, with a typical Dupal anomaly signature, is best represented by the young differentiated Kerguelen Archipelago lavas. The evolution with time of the relative proportions of the different components in the mix is reflected by the significant isotopic differences among the three sites sampled by Leg 121. Site 758 lavas have Sr, Nd, and Pb isotopic ratios closest to those of the Kerguelen Archipelago field, which may indicate a higher proportion of the hot-spot component in the mix than for the Site 756 lavas. The Site 216 samples have very low ϵ_{Nd} , low $^{206}\text{Pb}/^{204}\text{Pb}$, and high $^{87}\text{Sr}/^{86}\text{Sr}$ values (Dupré and Allègre, 1983; Mahoney et al., 1983), which is also consistent with a strong Kerguelen hot spot influence, maybe even stronger than for the Site 758 lavas. In the Pb-Pb isotope diagrams (Figs. 5 and 7), the Site 757 lavas are intermediate between the lavas of Sites 758 and 756. On the other hand, the input of a third component in the youngest lavas (i.e., at Site 756) from a St. Paul hot spot may also have had an important effect. The isotopic data reflect a change in tectonic setting between the >80-Ma-old lavas of Site 758 and >38-Ma-old lavas of Site 756. The Site 756 lavas are comparable in age to the older Kerguelen Archipelago lavas. They have Pb isotopic ratios intermediate between those of the Foch Island tholeiites and the Kerguelen transitional basalts, although with slightly higher $^{206}\text{Pb}/^{204}\text{Pb}$ ratios (Fig. 5). At this

time, there may have been a major source component derived from the spreading-ridge axis. The isotopic similarity of the Site 756 lavas to the young lavas erupted on the Southeast Indian Ridge from 33° to 37°S (Dosso et al., 1988) may reflect this proximity to the spreading ridge. An alternative explanation for the lower proportion of the Kerguelen hot spot component in the Site 756 lavas could be as follows. Spreading started along the Southeast Indian Ridge about 43 Ma (Schlich, 1982; Goslin and Patriat, 1984), in an east to west progression from 43 to 36 Ma (Royer and Sandwell, 1989), which is also the time when the first lavas started erupting on the Kerguelen Archipelago (Giret and Lameyre, 1983; Weis et al., 1989a; J. M. Cantagrel, pers. comm., 1990). Most of the magma generated by the hot spot at that time may have been drained by the building of the first massive tabular flows on the Kerguelen Islands on the Antarctic plate, on the southern side of the Southeast Indian Ridge. As a consequence, much less of the hot-spot component was available for the genesis of the southern tip of Ninetyeast Ridge, which was located on the northern side of the Southeast Indian Ridge. In contrast, the older lavas at Sites 758 and 216 overlap in isotopic ratios with the Kerguelen Archipelago field, relatively close to the Kerguelen hot spot, as represented by the young differentiated lavas of the southeast province, and that part of Ninetyeast Ridge may have formed when the hot spot and ridge axis did not exactly coincide.

Kerguelen and Heard islands record extensive histories of magmatic activity (in the case of Kerguelen Islands, from at least 42 Ma until the present; Giret and Lameyre, 1983; Nougier et al.,

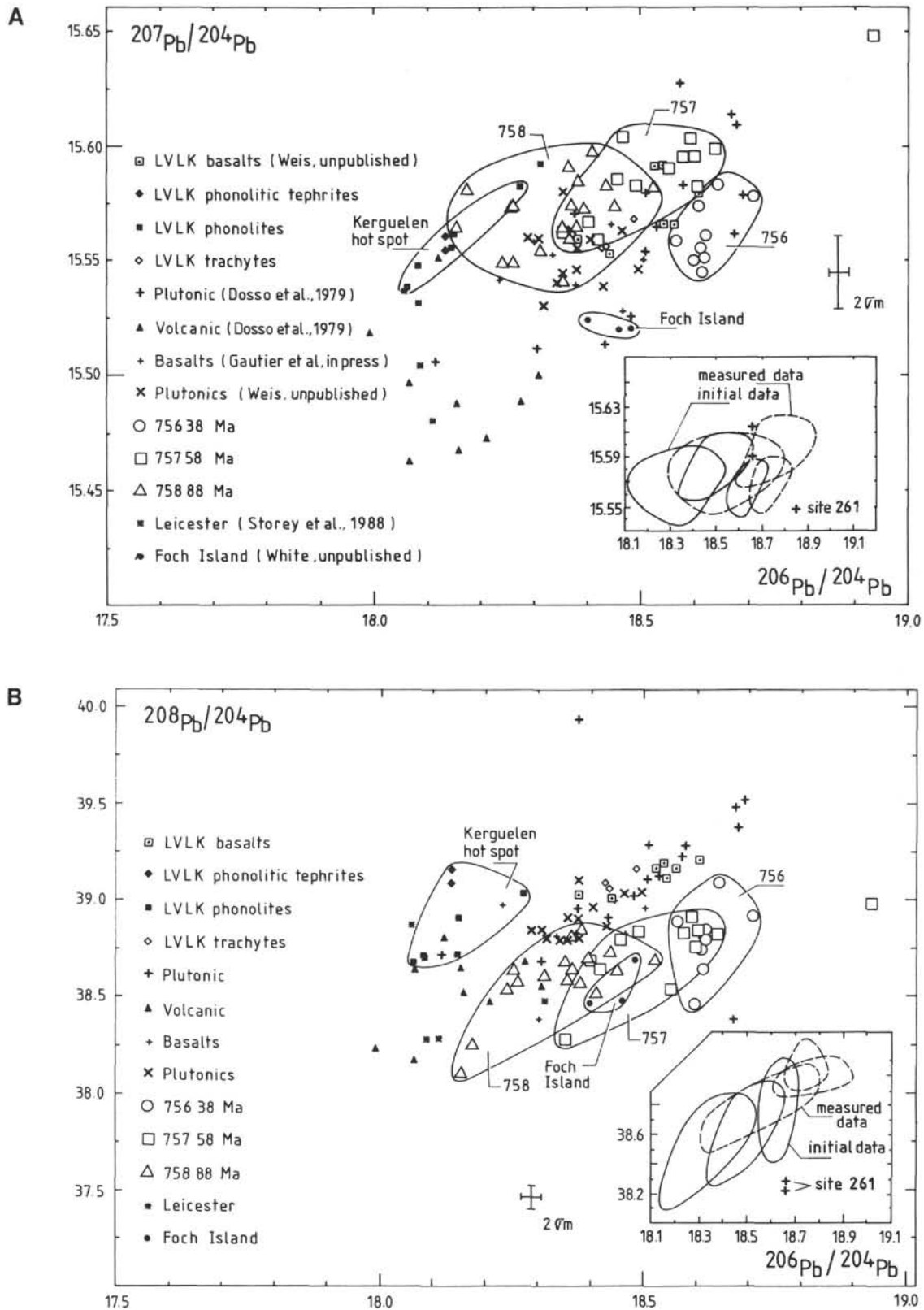


Figure 5. Detailed comparison of Pb isotopic ratios between the Leg 121 lavas (corrected for *in-situ* U and Th decay) and all data published for the Kerguelen Archipelago. References as in Figure 4, except for Dosso et al. (1979); Leicester data: Storey et al. (1988); plutonic rocks: Weis et al. (1987b) and D. Weis (unpubl. data); LVLK differentiated lavas: D. Weis (unpubl. data); and Foch Island tholeiites: W. M. White (pers. comm., 1985). **A.** $^{207}\text{Pb}/^{204}\text{Pb}$ vs. $^{206}\text{Pb}/^{204}\text{Pb}$. **B.** $^{208}\text{Pb}/^{204}\text{Pb}$ vs. $^{206}\text{Pb}/^{204}\text{Pb}$. Insets compare the measured (dashed line) and age-corrected for *in-situ* U and Th decay (solid line) Pb isotopic ratios for the lavas at each site. DSDP Site 261 data for ocean crust vein minerals from Hart and Staudigel (1986).

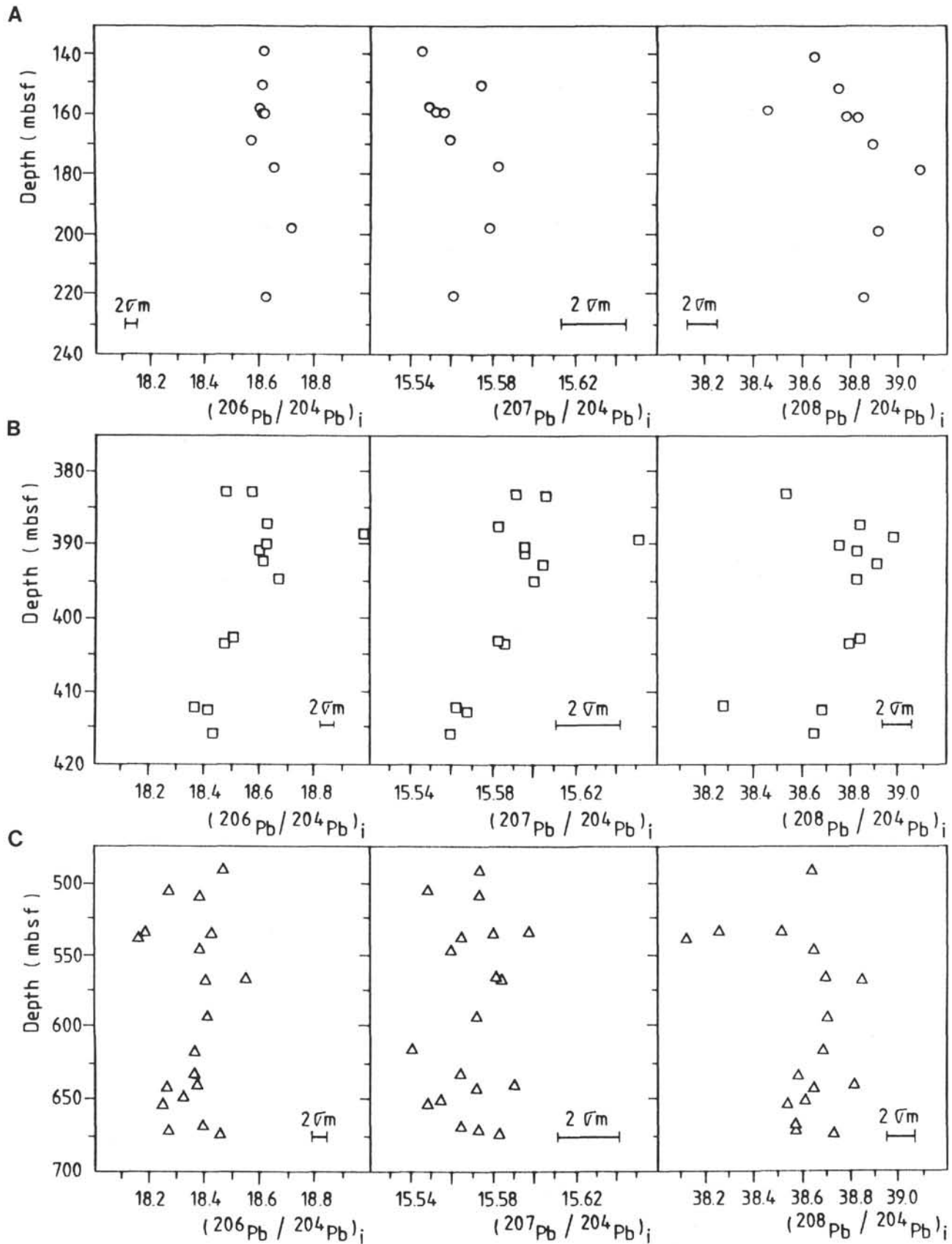


Figure 6. Age-corrected Pb isotopic ratios vs. depth. The horizontal scales are the same for comparison; the vertical ones differ. Symbols as in Figure 2 and age correction as in Figure 3. A. Site 756. B. Site 757. C. Site 758.

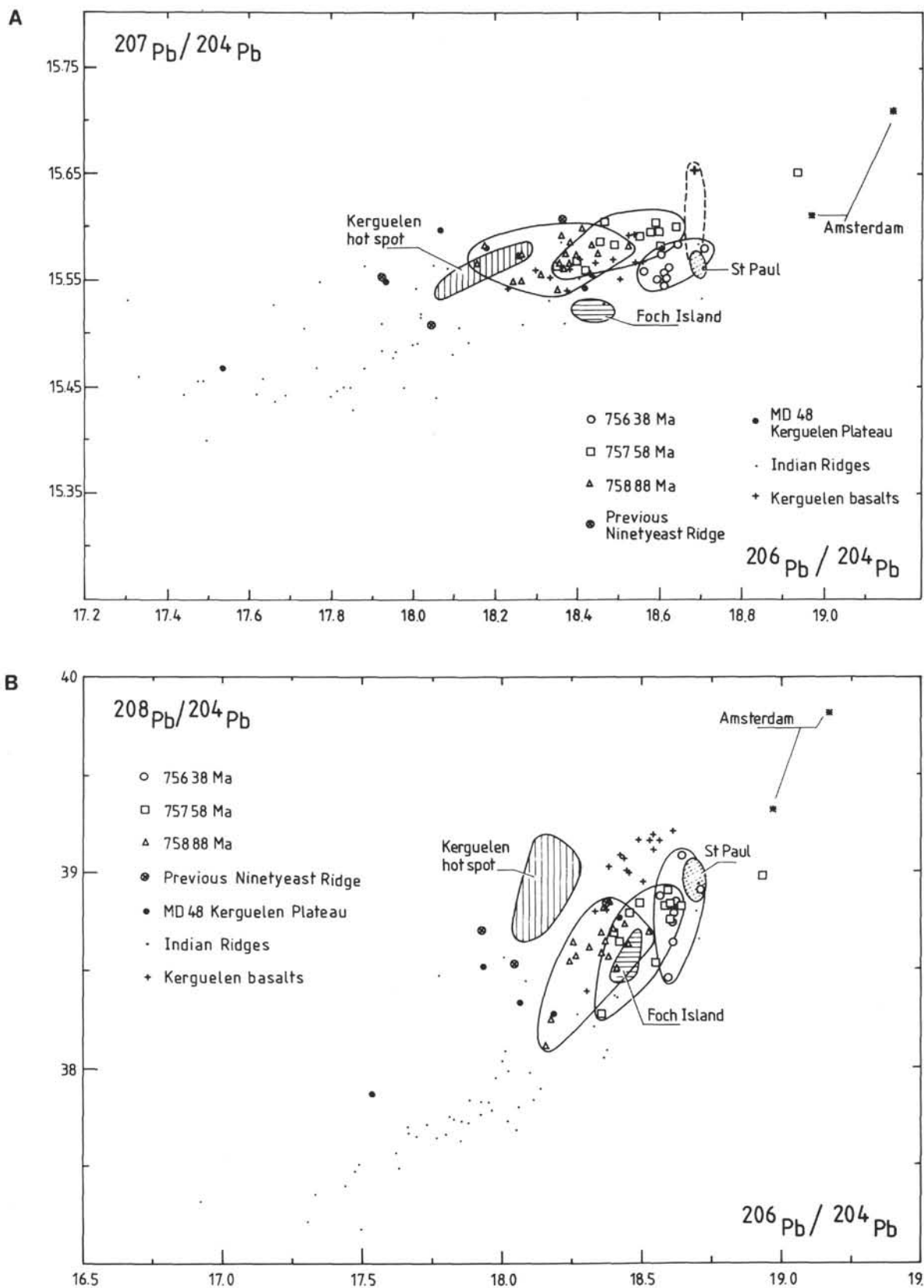


Figure 7. General comparison of Indian Ocean Pb isotopic ratios. Data sources as in Figures 4 and 5, except for St. Paul and Amsterdam islands (Dupré and Allègre, 1983; Hamelin et al., 1985/1986) and previous Ninetyeast Ridge data (Dupré and Allègre, 1983; Hart, 1988). A. $^{207}\text{Pb}/^{204}\text{Pb}$ vs. $^{206}\text{Pb}/^{204}\text{Pb}$. B. $^{208}\text{Pb}/^{204}\text{Pb}$ vs. $^{206}\text{Pb}/^{204}\text{Pb}$.

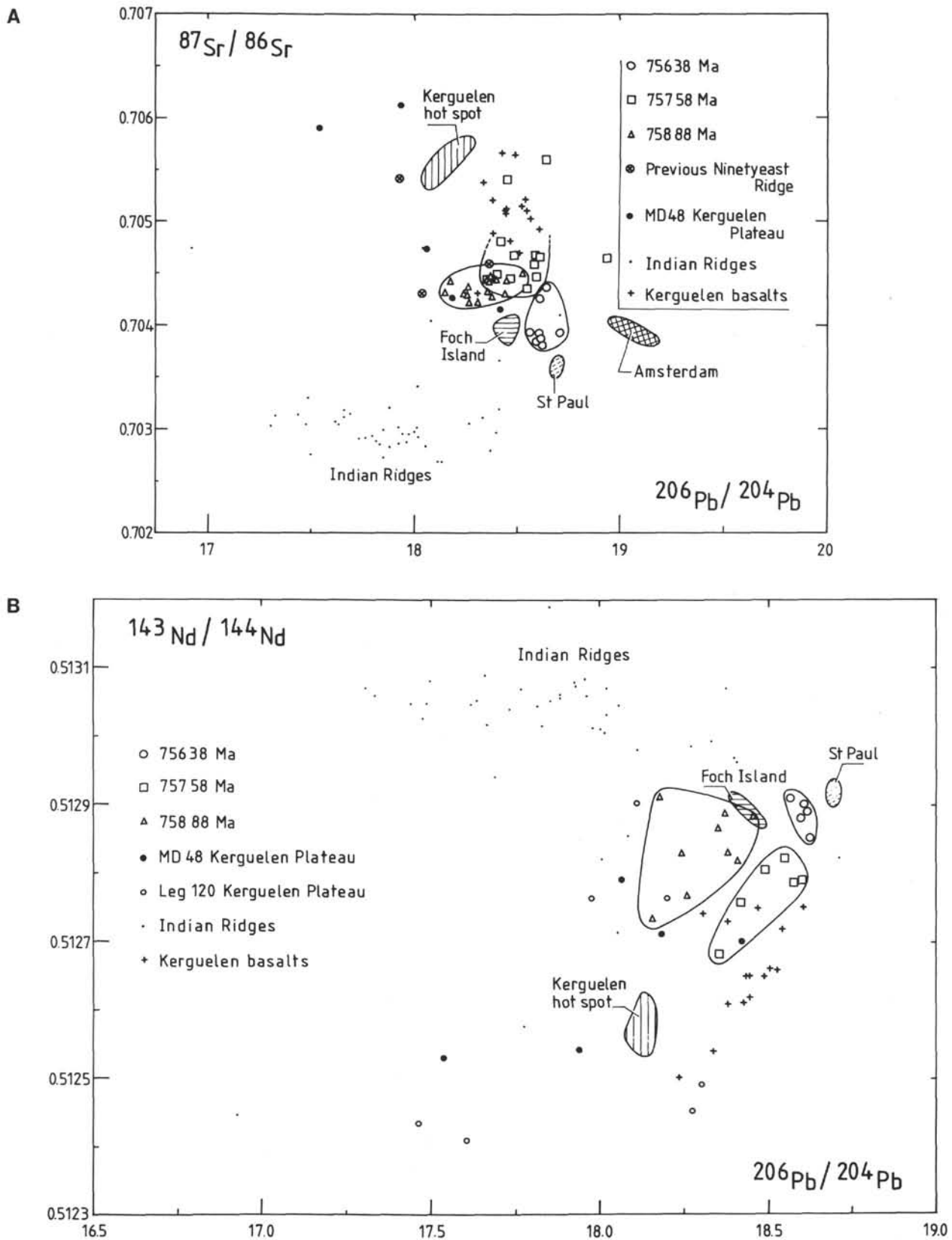


Figure 8. $^{87}\text{Sr}/^{86}\text{Sr}$ (A) and $^{143}\text{Nd}/^{144}\text{Nd}$ (B) vs. $^{206}\text{Pb}/^{204}\text{Pb}$. $^{87}\text{Sr}/^{86}\text{Sr}$ ratios are given for the leached samples of Leg 121 lavas and $^{143}\text{Nd}/^{144}\text{Nd}$ values are given for either unleached or leached samples according to the data reported in Table 3. $^{206}\text{Pb}/^{204}\text{Pb}$ values were corrected for *in-situ* ^{238}U decay under the assumption that U was not added recently from seawater. Data sources as in Figure 7.

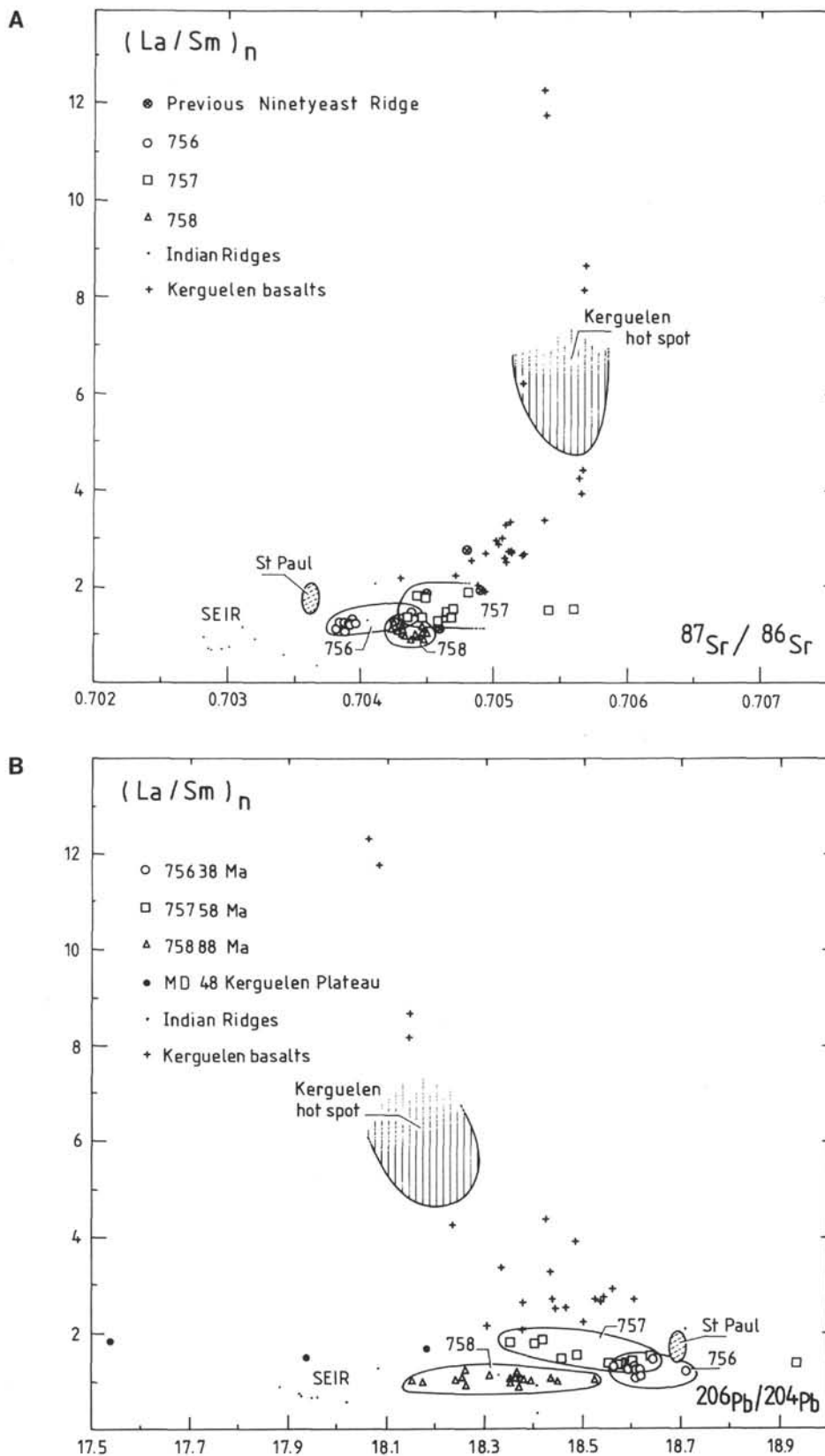


Figure 9. Trace element vs. isotopic ratio diagrams. Data sources as in Figure 7. A. $(La/Sm)_n$ (chondrite-normalized values from Sun and McDonough, 1989) vs. $^{87}Sr/^{86}Sr$ (present-day values of leached samples of the Leg 121 lavas). B. $(La/Sm)_n$ vs. $^{206}Pb/^{204}Pb$ (Leg 121 lavas corrected for *in-situ* ^{238}U decay).

1983). Despite important interisland variation, the basalts of the Kerguelen Archipelago have a strong Dupal signature, particularly in Pb and Sr isotope ratios (Weis et al., 1987b; Storey et al., 1988; Gautier et al., in press; D. Weis, unpubl. data). The involvement of the Kerguelen hot spot for at least 50 Ma in the genesis of the Ninetyeast Ridge lavas is evident from the isotopic data presented in this paper. Moreover, dredged samples from the Kerguelen Plateau, about 115 Ma old, also show a characteristic Dupal anomaly signature, although some are less pronounced than those of the Ninetyeast Ridge lavas and the Kerguelen Archipelago basalts, which may be indicative of a smaller relative proportion of the hot-spot component in the mixing process (Weis et al., 1989a). The origin of the Dupal component is uncertain. The isotopic and trace element characteristics of the Dupal OIBs are consistent with input from a subduction-related component—either subducted continental crust (e.g., as oceanic sediments; Hart, 1988; Sun and McDonough, 1989) or recycled subcontinental lithosphere (e.g., Allègre and Turcotte, 1985). A suitable model must account for the isolation of the different components for a significant amount of time, in either the subcontinental lithosphere, the continental crust, or deep in the mantle, in order to account for the large Pb isotope differences between the Dupal and non-Dupal OIBs.

The data from Ninetyeast Ridge and the Kerguelen Plateau show that the Kerguelen hot spot has been active more or less continuously for at least 115 Ma, even if the isotopic composition of erupted products has varied considerably, due to different relative proportions in the mixing process but also possibly due to heterogeneity in the hot spot itself. Intuitively, this seems to favor the hypothesis of a deep-seated origin for the Dupal anomaly. Moreover, the inferred seismic velocity distribution in the lower mantle shows that the Dupal anomaly maxima are located above large regions of low seismic velocity in the lower mantle (Hart, 1988; Castillo, 1988).

ACKNOWLEDGMENTS

The National Science Foundation (NSF), the Natural Environment Research Council (NERC, U.K.), the National Fund for Scientific Research (FNRS, Belgium), and the Research Council of Canada provided financial support for the petrologists on board. The project was organized and funded by the Ocean Drilling Program. We thank the Captain and the crew of the *SedcolBP 471* as well as the drilling staff and the ODP technician staff for their dedication.

The first author thanks the FNRS for allowing her participation on board and also for the financial support of the shorebased analyses (FRFC Convention no. 2.9002.90). Technical support was provided by Claire Chaval, Astrid Howard, and Jean-Paul Mennessier, who are thanked for their help, as well as the staff of the faculty department, who were very diligent in forwarding fax messages.

We very much appreciate the constructive review comments of the editor, J. Alt, and of J. Mahoney and W. M. White.

REFERENCES

- Allègre, C.-J., and Turcotte, D. L., 1985. Geodynamic mixing in the mesosphere boundary layer and the origin of oceanic islands. *Geophys. Res. Lett.*, 12:207–210.
- Barling, J., Goldstein, S. L., Wheller, G. E., and Nicholls, I. A., 1988. Heard Island: an example of large isotopic variations on a small oceanic island. *Chem. Geol.*, 70:46. (Abstract)
- Bowin, C., 1973. Origin of the Ninety East Ridge from studies near the equator. *J. Geophys. Res.*, 78:6029–6043.
- Cameron, A. E., Smith, D. H., and Walker, R. L., 1969. Mass spectrometry of nanogram-size samples of lead. *Anal. Chem.*, 41:525–526.
- Castillo, P., 1988. The Dupal anomaly as a trace of the upwelling lower mantle. *Nature*, 336:667–670.
- Catanzaro, E. J., Murphy, T. J., Shields, W. R., and Garner, E. L., 1968. Absolute isotopic abundance ratios of common, equal-atom, and radiogenic lead isotope standards. *J. Res. Natl. Bur. Stand.*, 72A:261–267.
- Curry, J. R., Emmel, F. J., Moore, D. G., and Raitt, R. W., 1982. Structure, tectonics and geological history of the northeastern Indian Ocean. In Nairn, A.E.M., and Stehli, F. G. (Eds.), *The Ocean Basins and Margins* (vol. 6): New York (Plenum), 399–450.
- Davies, H., Sun, S. S., Frey, F. A., Gautier, I., McCulloch, M. T., Price, R. C., Bassias, Y., Klootwijk, C. T., and Leclaire, L., 1989. Basalt basement from the Kerguelen Plateau and the trail of a Dupal plume. *Contrib. Mineral. Petrol.*, 103:457–469.
- Dosso, L., Bougault, H., Beuzart, P., Calvez, J.-Y., and Joron, J.-L., 1988. The geochemical structure of the South East Indian Ridge. *Earth Planet. Sci. Lett.*, 88:47–49.
- Dosso, L., and Murthy, R. V., 1980. A Nd isotopic study of the Kerguelen Islands: inferences on enriched oceanic mantle sources. *Earth Planet. Sci. Lett.*, 48:268–276.
- Dosso, L., Vidal, P., Cantagrel, J. M., Lameyre, J., Marot, A., and Zimine, S., 1979. Kerguelen: continental fragment or oceanic island?: petrology and isotopic geochemistry evidence. *Earth Planet. Sci. Lett.*, 43:46–60.
- Duncan, R. A., 1978. Geochronology of basalts from the Ninetyeast Ridge and continental dispersion in the eastern Indian Ocean. *J. Volcanol. Geotherm. Res.*, 4:283–305.
- Dupré, B., and Allègre, C.-J., 1983. Pb-Sr isotope variation in Indian Ocean basalts and mixing phenomena. *Nature*, 303:142–146.
- Frey, F. A., Dickey, J. S., Jr., Thompson, G., and Bryan, W. B., 1977. Eastern Indian Ocean DSDP sites: correlations between petrography, geochemistry and tectonic setting. In Heirtzler, J. R., and Sclater, J. G. (Eds.), *A Synthesis of Deep Sea Drilling in the Indian Ocean*: Washington (U.S. Govt. Printing Office), 189–257.
- Gautier, I., Frey, F. A., and Weis, D., 1989. The differentiated lavas of the Southeast Province of Kerguelen Archipelago (South Indian Ocean). *Eos, Trans. Am. Geophys. Union*, 70:1384. (Abstract)
- Gautier, I., Weis, D., Mennessier, J.-P., Vidal, P., Giret, A., and Loubet, M., 1990. Petrology and geochemistry of the Kerguelen Archipelago basalts: evolution of the mantle sources from ridge to intraplate position. *Earth Planet. Sci. Lett.* 100:59–76.
- Giret, A., and Lameyre, J., 1983. A study of Kerguelen plutonism: petrology, geochronology and geological implications. In Oliver, R. L., James, P. R., and Jago, J. B. (Eds.), *Antarctic Earth Science*: Cambridge (Cambridge Univ. Press), 646–651.
- Goslin, J., and Patriat, P., 1984. Absolute and relative plate motions and hypotheses on the origin of five aseismic ridges in the Indian Ocean. *Tectonophysics*, 101:221–244.
- Hamelin, B., and Allègre, C.-J., 1985. Large-scale regional units in the depleted upper mantle revealed by an isotope study of the South-West Indian Ridge. *Nature*, 315:196–199.
- Hamelin, B., Dupré, B., and Allègre, C.-J., 1985/1986. Pb-Sr-Nd isotopic data of Indian Ocean ridges: new evidence for large-scale mapping of mantle heterogeneities. *Earth Planet. Sci. Lett.*, 76:288–298.
- Hart, S. R., 1984. A large scale isotope anomaly in the Southern Hemisphere mantle. *Nature*, 309:753–757.
- , 1988. Heterogeneous mantle domains: signatures, genesis and mixing chronologies. *Earth Planet. Sci. Lett.*, 90:273–296.
- Hart, S. R., and Staudigel, H., 1986. Ocean crust vein mineral deposition: Rb/Sr ages, U-Th-Pb geochemistry, and duration of circulation at DSDP Sites 261, 462 and 516. *Geochim. Cosmochim. Acta*, 50:2751–2761.
- Leclaire, L., Denis-Clocchiatti, M., Davies, H. L., Gautier, I., Gensous, B., Giannesini, P. J., Morand, F., Patriat, P., Segoufin, J., Tesson, M., and Wannesson, J., 1987. Nature et âge du plateau de Kerguelen-Heard, secteur sud. Résultats préliminaires de la campagne "N.A.S.K.A.-MD48." *C. R. Acad. Sci., Ser. 2*, 304:23–28.
- Leg 121 Scientific Party, 1988. Leg 121 traces rifting and hot spots. *Geotimes*, 33:9–11.
- Leg 121 Shipboard Scientific Party, 1988. A tale of two ridges. *Nature*, 335:593–594.
- Le Roex, A. P., Dick, H.J.B., Erlank, A. J., Reid, A. M., Frey, F. A., and Hart, S. R., 1983. Geochemistry, mineralogy and petrogenesis of lavas erupted along the Southwest Indian Ridge between the Bouvet triple junction and 11 degrees East. *J. Petrol.*, 24:267–318.

- Luyendyk, B. P., and Rennick, W., 1977. Tectonic history of aseismic ridges in the eastern Indian Ocean. *Geol. Soc. Am. Bull.*, 88:1347–1356.
- MacDougall, J. D., 1977. Uranium in marine basalts: concentration, distribution and implications. *Earth Planet. Sci. Lett.*, 35:65–70.
- Mahoney, J. J., 1987. An isotopic survey of Pacific oceanic plateaus: implications for their nature and origin. In Keating, B. H., Fryer, P., Batiza, R., and Boehlert, G. W. (Eds.), *Seamounts, Islands, and Atolls*. Am. Geophys. Union Monogr., 43:207–220.
- Mahoney, J. J., MacDougall, J. D., Lugmair, G. W., and Gopalan, K., 1983. Kerguelen hotspot source for Rajmahal Traps and Ninetyeast Ridge? *Nature*, 303:385–389.
- Manhès, G., Minster, J.-F., and Allègre, C.-J., 1978. Comparative uranium-thorium-lead and rubidium-strontium of St. Severin amphoteric: consequences for early solar system chronology. *Earth Planet. Sci. Lett.*, 39:14–24.
- Michard, A., Montigny, R., and Schlich, R., 1986. Geochemistry of the mantle beneath the Rodriguez triple junction and the South-East Indian Ridge. *Earth Planet. Sci. Lett.*, 78:104–114.
- Molnar, P., and Stock, J., 1987. Relative motions of hot spots in the Pacific, Atlantic and Indian oceans since Late Cretaceous time. *Nature*, 327:587–591.
- Morgan, W. J., 1972. Deep mantle convection plumes and plate motions. *AAPG Bull.*, 56:203–213.
- Nougier, J., Pawlowski, D., and Cantagrel, J. M., 1983. Chrono-spatial evolution of the volcanic activity in southeastern Kerguelen (T.A.A.F.). In Oliver, R. L., James, P. R., and Jago, J. B. (Eds.), *Antarctic Earth Science*: Cambridge (Cambridge Univ. Press), 640–645.
- Peirce, J., Weissel, J., et al., 1989. *Proc. ODP, Init. Repts.*, 121: College Station, TX (Ocean Drilling Program).
- Peirce, J. W., 1978. The northward motion of India since the Late Cretaceous. *Geophys. J. R. Astron. Soc.*, 52:277–312.
- Price, R. C., Kennedy, A. K., Riggs-Sneeringer, M., and Frey, F. A., 1986. Geochemistry of basalts from the Indian Ocean triple junction: implications for the generation and evolution of Indian Ocean ridge basalts. *Earth Planet. Sci. Lett.*, 78:379–396.
- Royer, J.-Y., and Sandwell, D. T., 1989. Evolution of the eastern Indian Ocean since the Late Cretaceous: constraints from GEOSAT altimetry. *J. Geophys. Res.*, 94:13755–13782.
- Schlich, R., 1982. The Indian Ocean: aseismic ridges, spreading centers, and oceanic basins. In Nairn, A.E.M., and Stehli, F. G. (Eds.), *The Ocean Basins and Margins* (vol. 6): New York (Plenum), 51–147.
- Sclater, J. G., and Fisher, R. L., 1974. The evolution of the east central Indian Ocean with emphasis on the tectonic setting of the Ninetyeast Ridge. *Geol. Soc. Am. Bull.*, 85:683–702.
- Shipboard Scientific Party, 1974a. Site 215. In von der Borch, C. C., Sclater, J. G., et al., *Init. Repts. DSDP*, 22: Washington (U.S. Govt. Printing Office), 193–212.
- _____, 1974b. Site 256. In Davies, T. A., Luyendyk, B. P., et al., *Init. Repts. DSDP*, 26: Washington (U.S. Govt. Printing Office), 295–325.
- Storey, M., Saunders, A. D., Tarney, J., Leat, P., Thirlwall, M. F., Thompson, R. N., Menzies, M. A., and Marriner, G. F., 1988. Geochemical evidence for plume-mantle interactions beneath Kerguelen and Heard islands, Indian Ocean. *Nature*, 336:371–374.
- Sun, S.-S., and McDonough, W. F., 1989. Chemical and isotopic systematics of oceanic basalts: implications for mantle composition and processes. In Saunders, A. D., and Norry, M. J. (Eds.), *Magmatism in the Ocean Basins*. Geol. Soc. Spec. Publ. London, 42:313–345.
- Wasserburg, G. J., Jacobsen, S. B., DePaolo, D. J., McColloch, M., and Wen, T., 1981. Precise determination of Sm/Nd ratios, Sm and Nd isotopic abundances in standard solutions. *Geochim. Cosmochim. Acta*, 45:2311–2323.
- Weis, D., Bassias, Y., Gautier, I., and Mennesier, J.-P., 1989a. DUPAL anomaly in existence 115 Ma ago: evidence from isotopic study of the Kerguelen Plateau (South Indian Ocean). *Geochim. Cosmochim. Acta*, 53:2125–2131.
- Weis, D., Beaux, J.-F., Gautier, I., Giret, A., and Vidal, P., 1989b. Kerguelen Archipelago: geochemical evidence for recycled material. In Hart, S. R., and Gulen, L. (Eds.), *Crust/Mantle Recycling at Convergence Zones*: Amsterdam (Kluwer Academic Press), 59–63.
- Weis, D., Demaiffe, D., Cauët, S., and Javoy, M., 1987a. Sr, Nd, O and H isotopic ratios in Ascension lavas and plutonic inclusions: cogenetic origin. *Earth Planet. Sci. Lett.*, 82:316–322.
- Weis, D., Frey, F. A., Saunders, A. D., Gibson, I., and Leg 121 Scientific Shipboard Party, 1991. The Ninetyeast Ridge (Indian Ocean): a 5000 km record of a DUPAL mantle plume. *Geology*, 19:99–102.
- Weis, D., Mennesier, J.-P., Gautier, I., Cantagrel, J.-M., and Vidal, P., 1987b. Géochimie isotopique des Terres Australes (Archipel des îles Kerguelen). *Actes Coll. Recherche Française dans les Terres Australes*. Strasbourg (CNFRA), 357–368.
- White, W. M., 1985. Source of oceanic basalts: radiogenic isotope evidence. *Geology*, 13:519–523.
- White, W. M., and Hofmann, A. W., 1982. Sr and Nd isotope geochemistry of oceanic basalts and mantle evolution. *Nature*, 296:821–825.
- Whitford, D. J., and Duncan, R. A., 1978. Origin of the Ninetyeast Ridge—Sr isotope and trace element evidence. In Zartman, R. E. (Ed.), *Short Papers of the Fourth International Conference, Geochronology, Cosmochronology, Isotope Geology*. Open-File Rep. U.S. Geol. Surv., 78-701:451–453.
- Zindler, A., and Hart, S., 1986. Chemical geodynamics. *Annu. Rev. Earth Planet. Sci.*, 14:493–571.

Date of initial receipt: 16 March 1990
Date of acceptance: 12 November 1990
Ms 121B-170